

Model-independent measurement of charm mixing parameters in $\bar{B} \rightarrow D^0(\rightarrow K_S^0\pi^+\pi^-)\mu^-\bar{\nu}_\mu X$ decays

R. Aaij *et al.**
(LHCb Collaboration)

 (Received 16 August 2022; accepted 7 October 2022; published 6 September 2023)

A measurement of charm mixing and CP -violating parameters is reported, using $\bar{B} \rightarrow D^0(\rightarrow K_S^0\pi^+\pi^-)\mu^-\bar{\nu}_\mu X$ decays reconstructed in proton-proton collisions collected by the LHCb experiment during the years 2016 to 2018, corresponding to an integrated luminosity of 5.4 fb^{-1} . The measured mixing and CP -violating parameters are $x_{CP} = [4.29 \pm 1.48(\text{stat}) \pm 0.26(\text{syst})] \times 10^{-3}$, $y_{CP} = [12.61 \pm 3.12(\text{stat}) \pm 0.83(\text{syst})] \times 10^{-3}$, $\Delta x = [-0.77 \pm 0.93(\text{stat}) \pm 0.28(\text{syst})] \times 10^{-3}$, $\Delta y = [3.01 \pm 1.92(\text{stat}) \pm 0.26(\text{syst})] \times 10^{-3}$. The results are complementary to and consistent with previous measurements. A combination with the recent LHCb analysis of $D^{*+} \rightarrow D^0(\rightarrow K_S^0\pi^+\pi^-)\pi^+$ decays is reported.

DOI: [10.1103/PhysRevD.108.052005](https://doi.org/10.1103/PhysRevD.108.052005)

I. INTRODUCTION

Flavor oscillation is the transition between a neutral flavored meson and its antiparticle. In the Standard Model (SM) of particle physics, this transition is mediated by charged-current weak interactions, involving the exchange of two virtual W bosons. A contribution from unknown massive virtual particles could interfere with the SM oscillation amplitude. This phenomenon is hence sensitive to physics beyond the SM at large scales [1].

The oscillation occurs because the quark mass terms in the SM Lagrangian cannot be simultaneously diagonalized with the weak coupling terms. The mass eigenstates of the neutral charm meson can be written as linear combinations of the flavor eigenstates as $|D_{1,2}\rangle = p|D^0\rangle \pm q|\bar{D}^0\rangle$, where p and q are complex parameters satisfying the normalization condition $|p|^2 + |q|^2 = 1$. The quantities $m_{1,2}$ and $\Gamma_{1,2}$ are the mass and decay width of the $D_{1,2}$ states, respectively. The oscillation can be described with two dimensionless parameters,

$$x = (m_1 - m_2)c^2/\Gamma, \quad (1)$$

$$y = (\Gamma_1 - \Gamma_2)/(2\Gamma), \quad (2)$$

where $\Gamma = (\Gamma_1 + \Gamma_2)/2$ is the average decay width.

In this formalism, CP violation in mixing can manifest itself through a deviation of $|q/p|$ from unity. If the D^0 and \bar{D}^0 mesons decay to a common final state f , a nonzero

phase $\phi_f \equiv \arg(q\bar{A}_f/pA_f)$ can arise from CP violation in the interference between mixing and decay. Here, A_f (\bar{A}_f) denotes the $D^0 \rightarrow f$ ($\bar{D}^0 \rightarrow f$) decay amplitude. If CP symmetry is conserved in the decay amplitude, the CP -violating phase is final-state independent and denoted as ϕ .

The parameters of interest are expressed in terms of the CP -averaged mixing parameters

$$x_{CP} = \frac{1}{2} \left[x \cos \phi \left(\left| \frac{q}{p} \right| + \left| \frac{p}{q} \right| \right) + y \sin \phi \left(\left| \frac{q}{p} \right| - \left| \frac{p}{q} \right| \right) \right], \quad (3)$$

$$y_{CP} = \frac{1}{2} \left[y \cos \phi \left(\left| \frac{q}{p} \right| + \left| \frac{p}{q} \right| \right) - x \sin \phi \left(\left| \frac{q}{p} \right| - \left| \frac{p}{q} \right| \right) \right], \quad (4)$$

and the CP -violating differences

$$\Delta x = \frac{1}{2} \left[x \cos \phi \left(\left| \frac{q}{p} \right| - \left| \frac{p}{q} \right| \right) + y \sin \phi \left(\left| \frac{q}{p} \right| + \left| \frac{p}{q} \right| \right) \right], \quad (5)$$

$$\Delta y = \frac{1}{2} \left[y \cos \phi \left(\left| \frac{q}{p} \right| - \left| \frac{p}{q} \right| \right) - x \sin \phi \left(\left| \frac{q}{p} \right| + \left| \frac{p}{q} \right| \right) \right]. \quad (6)$$

Absence of CP violation ($|q/p| = 1$, $\phi = 0$) implies $x_{CP} = x$, $y_{CP} = y$, and $\Delta x = \Delta y = 0$.

Oscillations in the K and B meson systems are well established [2–5]. The evidence and observation of D^0 – \bar{D}^0 oscillations were reported much later by the *BABAR* [6], *Belle* [7] and LHCb [8] collaborations, because of the small oscillation probability governed by the size of the x and y parameters. The value of x has only recently been measured to significantly differ from zero [9]. Moreover, CP violation in the charm sector has been experimentally confirmed much later than in the K and B meson systems. To date, only a single measurement with significance

*Full author list given at the end of the article.

Published by the American Physical Society under the terms of the [Creative Commons Attribution 4.0 International license](https://creativecommons.org/licenses/by/4.0/). Further distribution of this work must maintain attribution to the author(s) and the published article's title, journal citation, and DOI. Funded by SCOAP³.

greater than 5σ exists [10] for the difference in time-integrated CP violation in $D^0 \rightarrow K^-K^+$ and $D^0 \rightarrow \pi^-\pi^+$ decays.¹ There have been no experimental indications of CP violation in mixing or in the interference between mixing and decay of neutral charm mesons thus far. The current world averages of mixing and CP -violating parameters are [11]

$$\begin{aligned} x &= (0.409_{-0.049}^{+0.048}) \times 10^{-2}, \\ y &= (0.615_{-0.055}^{+0.056}) \times 10^{-2}, \\ |q/p| &= 0.995 \pm 0.016, \\ \phi &= -0.044 \pm 0.021 \text{ rad.} \end{aligned}$$

The self-conjugate decay $D^0 \rightarrow K_S^0\pi^+\pi^-$ provides direct access to both the charm mixing and CP -violating parameters. Using this decay, with the D^0 produced in the decay chain $D^{*+} \rightarrow D^0(\rightarrow K_S^0\pi^+\pi^-)\pi^+$, the LHCb collaboration reported the first observation of a nonzero value for the x parameter [9].

This paper presents a measurement of charm mixing parameters in $D^0 \rightarrow K_S^0\pi^+\pi^-$ decays reconstructed in proton-proton (pp) collision data, collected by the LHCb experiment between 2016 and 2018 (Run 2), corresponding to an integrated luminosity of 5.4 fb^{-1} . The D^0 mesons originate from semileptonic decays of b hadrons of the form $\bar{B} \rightarrow D^0(\rightarrow K_S^0\pi^+\pi^-)\mu^-\bar{\nu}_\mu X$, where the D^0 flavor is determined from the charge of the muon. The measurement is based on the so-called *bin-flip* approach, an improved model-independent method, based on [12,13], that suppresses biases due to a nonuniform event reconstruction efficiency as a function of phase space and decay-time [14]. This measurement complements the above-mentioned analysis of $D^{*+} \rightarrow D^0(\rightarrow K_S^0\pi^+\pi^-)\pi^+$ decays [9]. The independent data sample of D^0 mesons from semileptonic decays allows to sample the low decay-time region, which is not accessible to the $D^{*+} \rightarrow D^0(\rightarrow K_S^0\pi^+\pi^-)\pi^+$ decays analysis. The procedure of the analysis presented here is mostly aligned with that reported in Ref. [9]. A combination of the two results is performed to exploit the increased data sample size and wider coverage of D^0 decay-time.

II. THE LHCb DETECTOR

The LHCb detector [15,16] is a single-arm forward spectrometer covering the pseudorapidity range $2 < \eta < 5$, designed for the study of particles containing b or c quarks. The detector includes a high-precision tracking system consisting of a silicon-strip vertex detector surrounding the pp interaction region, a large-area silicon-strip detector located upstream of a dipole magnet with a bending power of about 4 Tm, and three stations of silicon-strip detectors

and straw drift tubes placed downstream of the magnet. The tracking system provides a measurement of the momentum, p , of charged particles with a relative uncertainty that varies from 0.5% at low momentum to 1.0% at 200 GeV/ c . The minimum distance of a track to a primary pp collision vertex (PV), the impact parameter (IP), is measured with a resolution of $(15 + 29/p_T) \mu\text{m}$, where p_T is the component of the momentum transverse to the beam, in GeV/ c . Different types of charged hadrons are distinguished using information from two ring-imaging Cherenkov detectors. Photons, electrons and hadrons are identified by a calorimeter system consisting of scintillating-pad and pre-shower detectors, an electromagnetic and a hadronic calorimeter. Muons are identified by a system composed of alternating layers of iron and multiwire proportional chambers. The online event selection is performed by a trigger, which consists of a hardware stage, based on information from the calorimeter and muon systems, followed by a software stage, which applies a full event reconstruction.

Simulation is required to model the effects of the detector acceptance and the imposed selection requirements. In the simulation, pp collisions are generated using PYTHIA [17] with a specific LHCb configuration [18]. Decays of unstable particles are described by EvtGen [19], in which final-state radiation is generated using PHOTOS [20]. The interaction of the generated particles with the detector, and its response, are implemented using the Geant4 toolkit [21] as described in Ref. [22].

III. ANALYSIS METHOD

The analysis is based on the bin-flip method proposed in Ref. [14]. It is a model-independent approach, optimized for the measurement of the mixing parameter x , which avoids the need for an accurate modeling of the efficiency variation across phase space and decay-time. The relevant aspects of the method are summarized below.

The $D^0 \rightarrow K_S^0\pi^+\pi^-$ decay dynamics is embodied in a Dalitz plot, parametrized with the squared two-body masses,

$$m_{\pm}^2 \equiv \begin{cases} m^2(K_S^0\pi^{\pm}) & \text{for } D^0 \rightarrow K_S^0\pi^+\pi^- \text{ decays} \\ m^2(K_S^0\pi^{\mp}) & \text{for } \bar{D}^0 \rightarrow K_S^0\pi^+\pi^- \text{ decays} \end{cases}. \quad (7)$$

The parameters of interest are obtained from time-dependent ratios of yields in bins symmetric with respect to the principal bisector of the Dalitz plot, which is defined by $m_+^2 = m_-^2$. The region defined by $m_+^2 > m_-^2$ ($m_+^2 < m_-^2$) is called the lower (upper) region of the Dalitz plot. Among possible intermediate resonances, the D^0 meson decay can proceed through a Cabibbo-favored (CF) path via $K^{*-}\pi^+$ or a doubly Cabibbo-suppressed (DCS) path via $K^{*+}\pi^-$.

These paths populate specific regions in the Dalitz plot, as can be seen in Fig. 1 (left). The decays proceeding through the CF path dominate in the lower part of the Dalitz

¹Charge conjugation is implied throughout the paper.

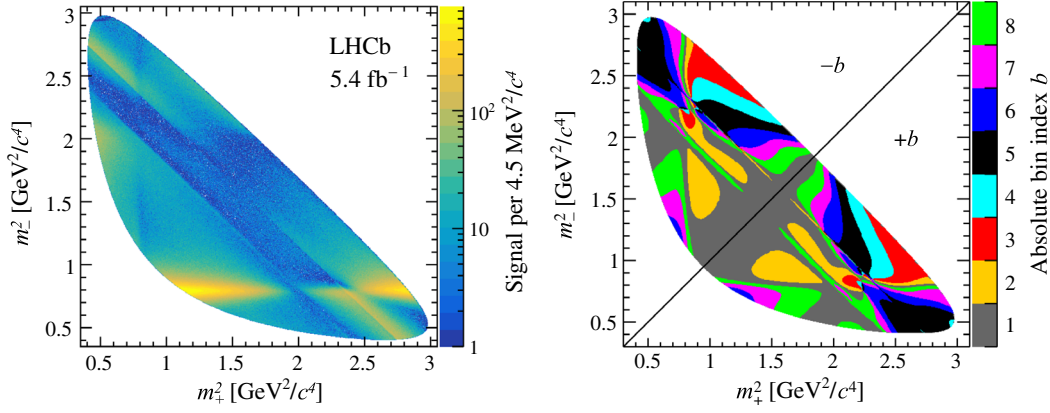


FIG. 1. (Left) D^0 Dalitz plot of reconstructed $\bar{B} \rightarrow D^0(\rightarrow K_S^0\pi^+\pi^-)\mu^-\bar{\nu}_\mu X$ decays for the D^0 flavor and (right) definition of the binning scheme proposed by CLEO [23].

plot, while the DCS transitions populate the upper part of the plot. The ratio of decays in these two regions of the Dalitz plot does not change with time in the absence of mixing. In the presence of mixing, the D^0 mesons that have oscillated and decay via the CF path populate the same region as nonmixed mesons decaying via the DCS path. Measuring the time evolution of the ratio between the yields in those regions gives access to the mixing parameters. Separating the data sample by flavor further allows the measurement of CP -violating parameters.

The Dalitz space is divided into bins such that each bin b in the lower part of the Dalitz plot has a corresponding bin $-b$ in the upper part of the Dalitz plot.

A scheme with eight pairs of bins as proposed by CLEO [23] is used, where bins are chosen such that the strong phase difference between the D^0 and \bar{D}^0 amplitudes is nearly constant in each bin. The binning scheme is depicted in Fig. 1 (right). The data are further divided into ten equipopulated bins with the following edges in the measured D^0 decay-time,

$$[0.00, 0.155, 0.285, 0.42, 0.57, 0.74, 0.94, 1.20, 1.58, 2.22, 20.00]\tau_{D^0}, \quad (8)$$

where τ_{D^0} is the world-average value of the D^0 lifetime [5]. The yields are measured for each initial flavor of the D^0 meson, Dalitz bin and decay-time bin.

For small mixing parameters and in the limit of CP -conserving decay amplitudes, the ratio of yields between the Dalitz bin $-b$ and the Dalitz bin $+b$ in the decay-time bin j can be expressed as [14]

$$R_{bj}^\pm \approx \frac{r_b + \frac{1}{4}r_b\langle t^2 \rangle_j \text{Re}\left(z_{CP}^2 - \Delta z^2 + \frac{1}{4}\langle t^2 \rangle_j |z_{CP} \pm \Delta z|^2 + \sqrt{r_b}\langle t \rangle_j\right) \text{Re}[X_b^*(z_{CP} \pm \Delta z)]}{1 + \frac{1}{4}\langle t^2 \rangle_j \text{Re}\left(z_{CP}^2 - \Delta z^2 + r_b \frac{1}{4}\langle t^2 \rangle_j |z_{CP} \pm \Delta z|^2 + \sqrt{r_b}\langle t \rangle_j\right) \text{Re}[X_b(z_{CP} \pm \Delta z)]}, \quad (9)$$

where the $+$ ($-$) sign refers to the D^0 (\bar{D}^0) initial flavor. Here $\langle t \rangle_j$ ($\langle t^2 \rangle_j$) is the average of the decay-time (squared) of unmixed decays in units of τ_{D^0} , r_b is the decay-time independent ratio of signal yields between bins $-b$ and $+b$, $z_{CP} \pm \Delta z \equiv -(q/p)^{\pm 1}(y + ix)$, and $X_b \equiv c_b - is_b$, where c_b and s_b are the amplitude-weighted averages of the cosine and sine of the strong-phase difference over the Dalitz bin $\pm b$. The mixing and CP -violating parameters are determined by performing a simultaneous fit of the R_{bj}^\pm expressions to the measured yield ratios. Equation (9) is valid if time-dependent variations of the Dalitz plot efficiency are negligible. Time-independent efficiency

variations in the Dalitz phase space do not affect the extraction of the mixing and CP -violating parameters, which relate to z_{CP} and Δz as

$$x_{CP} = -\text{Im}(z_{CP}), \quad \Delta x = -\text{Im}(\Delta z), \quad (10)$$

$$y_{CP} = -\text{Re}(z_{CP}), \quad \Delta y = -\text{Re}(\Delta z). \quad (11)$$

The analysis steps are described in the following paragraphs, with references to specific sections given where applicable. Section IV explains the initial selection of the data, which includes a multivariate analysis (MVA)

dedicated to the suppression of the combinatorial background. The bin-flip method assumes no correlation between decay-time and Dalitz-space coordinates, as it integrates over Dalitz and decay-time bins separately. Experimentally induced correlations, caused by nonuniform selection efficiencies, are removed through a combination of simulation-based and data-driven methods, which is described in detail in Sec. V. Validation tests are performed to confirm that any remaining reconstruction and selection effects do not affect the final result and hence do not need to be explicitly accounted for. These studies are later used to construct realistic pseudoexperiment models for the study of systematic uncertainties.

The data, weighted according to the decorrelation method, are split into bins of Dalitz space and decay-time, and separated according to the D^0 meson initial flavor. The data are further categorized as LL or DD depending on whether the K_S^0 meson decay products are reconstructed as long or downstream tracks. Long tracks are reconstructed from hits in both the VELO and the downstream tracking stations. Downstream tracks do not use any hit information from the VELO. The data is not split by data-taking year or magnet polarity, and cross-checks are performed to validate that there is no dependence of the results on data taking conditions.

Unbinned maximum likelihood fits to the invariant-mass distribution of the reconstructed D^0 mesons are performed for each category and bin to extract the signal yields. The fit model includes signal and combinatorial background components. The signal is described by a sum of a Johnson SU function [24] and a bifurcated Gaussian function. The combinatorial background is modeled with a first-order (second-order) Chebyshev polynomial for the K_S^0 LL (DD) category.

Equation (9) requires as inputs the averages of $t = \tau/\tau_{D^0}$ and t^2 in each time bin j , where τ is the proper decay-time and τ_{D^0} the average D^0 lifetime. They are computed as

$$\langle t \rangle_j = \frac{\sum_i w_i t_i}{\sum_i w_i} \quad \text{and} \quad \langle t^2 \rangle_j = \frac{\sum_i w_i t_i^2}{\sum_i w_i}, \quad (12)$$

where the sum is over the selected candidates i in decay-time bin j and in the lower part of the Dalitz plot (as this area is dominated by decays of mesons that did not undergo mixing), and w_i is the product of a signal weight obtained from the mass fit using the *sPlot* method [25] and a weight from the decorrelation procedure.

The mixing and CP -violating parameters are determined using a least-squares fit of the R_{bj}^\pm expressions of Eq. (9) to the $2 \times 2 \times 8 \times 10 \times 2 = 640$ measured yields $N_{\pm bjk}^\pm$ and their uncertainties $\sigma_{\pm bjk}^\pm$ in all bins and categories. The χ^2 function

$$\chi^2 = \sum_b^8 \sum_j^{10} \sum_{k=LL,DD} \left[\frac{(N_{-bjk}^+ - N_{+bjk}^+ R_{bj}^+)^2}{(\sigma_{-bjk}^+)^2 + (\sigma_{+bjk}^+ R_{bj}^+)^2} + \frac{(N_{-bjk}^- - N_{+bjk}^- R_{bj}^-)^2}{(\sigma_{-bjk}^-)^2 + (\sigma_{+bjk}^- R_{bj}^-)^2} \right] + \chi_X^2 \quad (13)$$

is minimized, where the Gaussian penalty term

$$\chi_X^2 = \sum_b^8 \sum_{b'}^8 (X_b^{\text{ext}} - X_b)(V_{\text{ext}}^{-1})_{bb'}(X_{b'}^{\text{ext}} - X_{b'}) \quad (14)$$

represents external constraints on the eight complex quantities X_b from the combined determinations X_b^{ext} (with statistical and systematic covariance matrix V_{ext}) of the CLEO and BESIII measurements [26].

The free parameters of the χ^2 minimization are $x_{CP}, y_{CP}, \Delta x, \Delta y$, and the eight ratios r_b . The results are presented in Sec. VII.

The systematic uncertainties are discussed in Sec. VI. They are determined using generated pseudoexperiments that apply reconstruction and selection effects to an amplitude model in order to obtain a realistic description of the data.

This analysis complements the measurement of mixing and CP -violating parameters with the bin-flip method using D^0 mesons from the decay chain $D^{*+} \rightarrow D^0(\rightarrow K_S^0 \pi^+ \pi^-) \pi^+$ [9]. Section VIII presents a combination of the two sets of results, which is done by performing a simultaneous fit to the two samples.

IV. CANDIDATE SELECTION

Candidates are reconstructed in the decay chain $\bar{B} \rightarrow D^0(\rightarrow K_S^0 \pi^+ \pi^-) \mu^- \bar{\nu}_\mu X$, where X represents possible additional decay products that are not reconstructed. The K_S^0 candidates are reconstructed from two oppositely charged pion tracks either in the LL or DD category (see Sec. III). At least one displaced, high-transverse-momentum muon is required. An MVA algorithm is used to select candidates conforming to a topology of an n -body ($n = 2, 3, 4$) decay of a b -hadron, where at least one of the tracks must be a muon. A fit [27] is then performed on the selected candidates, constraining the D^0 decay tracks to a common origin vertex and the K_S^0 mass to its world average value [5]. The analysis uses the reconstructed D^0 mass $m(K_S^0 \pi^+ \pi^-)$ and decay-time variables obtained from this fit. The Dalitz-plot coordinates are determined in another fit in which the D^0 mass is constrained to its known value [5].

Combinatorial background is further suppressed with a dedicated MVA, namely a boosted decision tree (BDT) classifier [28]. The signal and background distributions for the training are obtained through the *sPlot* technique using the fit to the $m(K_S^0 \pi^+ \pi^-)$ distribution. The signal range is

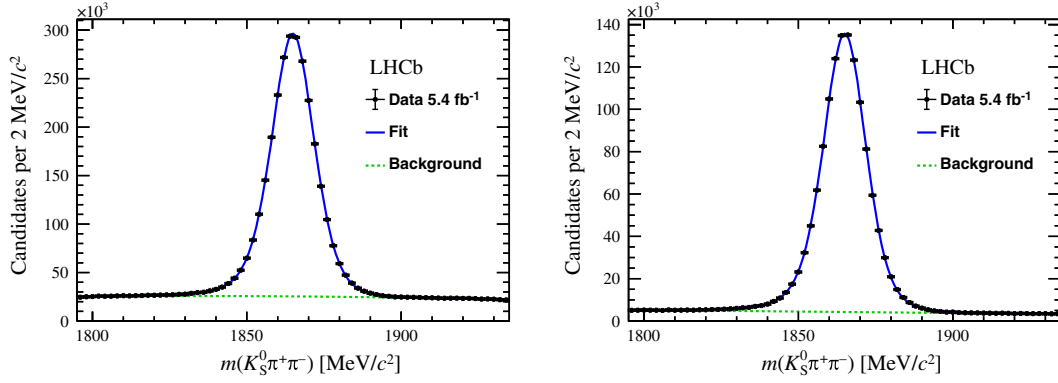


FIG. 2. $K_S^0\pi^+\pi^-$ invariant-mass distribution of (left) DD and (right) LL K_S^0 candidates after all selection requirements, with fit results superimposed.

[1795, 1935] MeV/c^2 . The BDT employs topological and kinematic variables related to the reconstructed b hadron: the quality of the primary and secondary vertices, the difference in the vertex-fit χ^2 of the PV reconstructed with and without the decay products of the b -hadron, the flight distance, the cosine of the angle between the momentum and the vector connecting the primary and secondary vertices, and the corrected mass $m_{\text{corr}} = \sqrt{m^2(D^0\mu^-) + p_{\perp}^2(D^0\mu^-) + p_{\perp}(D^0\mu^-)}$, where $m(D^0\mu^-)$ is the invariant mass of the $D^0\mu^-$ combination and $p_{\perp}(D^0\mu^-)$ is the component of its momentum perpendicular to the b hadron flight direction. The only variables related to the b -hadron children are the transverse momenta of the muon and the reconstructed D^0 meson. A gradient boosting algorithm is used with uniform regularization (uBoost) [29]. A manual 6-fold cross-validation is implemented [30].

A requirement on the BDT output variable is optimized by maximizing the signal significance, defined as $N_{\text{sig}}/\sqrt{N_{\text{sig}} + N_{\text{bkg}}}$, where N_{sig} and N_{bkg} are the numbers of signal and background events, obtained from fits to the D^0 mass distribution. The optimal points are computed separately for each K_S^0 category. Validation tests support the strategy of using a single value for all data-taking years. The selection retains 80% (73%) of the signal candidates and increases the signal purity from 26% (21%) to 79% (59%) for the LL (DD) sample. Duplicated tracks that originate from the same physical particle are removed for the LL sample by rejecting candidates using tracks for which the slope in the VELO is too similar to that of another track in the event. For the DD sample, in addition to the requirement on the track slopes, a large enough difference in the reconstructed momentum is required for any two tracks. If there are multiple candidates in the event after the clone tracks removal, a single randomly chosen candidate is retained.

The yields are extracted through a fit to $m(K_S^0\pi^+\pi^-)$ distribution. The total signal yields after the full selection

are 1.24×10^6 (2.48×10^6) for the LL (DD) sample. The $K_S^0\pi^+\pi^-$ invariant-mass distribution after the selection is shown in Fig. 2, with fit results superimposed.

V. DECORRELATION

An important assumption of the analysis method is that there are no experimentally induced correlations between phase-space coordinates and the D^0 candidate decay-time, such that it is possible to integrate separately over the Dalitz bins and in bins of decay-time to obtain the decay-time-independent coefficients r_b and X_b .

Such a correlation has already been observed in the analysis of the decay $D^{*+} \rightarrow D^0(\rightarrow K_S^0\pi^+\pi^-)\pi^+$ [9,31]. In this data sample, it is induced mainly by the online software selection for n -body hadronic b hadron decays ($n = 2, 3, 4$) [32]. The selection requires that 2, 3 or 4 tracks form a single displaced vertex. In the case of $\bar{B} \rightarrow D^0(\rightarrow K_S^0\pi^+\pi^-)\mu^-\bar{\nu}_\mu X$, one of the tracks is required to be a muon, and all other tracks must come from the children of the D^0 meson. Hence, the selection favors configurations where the D^0 meson decays close to the B -meson vertex, introducing a correlation between the Dalitz coordinates and the D^0 decay-time. This is shown in Fig. 3, where the dependence of the squared invariant mass of the two final-state pions, $m^2(\pi^+\pi^-)$, on the normalized D^0 meson decay-time τ/τ_{D^0} is reported. The figure shows the signal yields, normalized to the maximum yield, in each $m^2(\pi^+\pi^-)$ bin as a function of D^0 decay-time. Due to the known small values of the mixing parameters [11] and the $D^0 \rightarrow K_S^0\pi^+\pi^-$ amplitude model [33], the correlation between $m^2(\pi^+\pi^-)$ and the D^0 decay-time caused by the mixing effect is negligible at the current sample size.

Therefore, the correlation observed in Fig. 3 is induced by the online software selection only.

Using $\bar{B} \rightarrow D^0(\rightarrow K_S^0\pi^+\pi^-)\mu^-\bar{\nu}_\mu X$ simulated events, the efficiency of the online selection is determined as a function of the D^0 decay-time, $m^2(\pi^+\pi^-)$ and $\cos\theta_{\pi^+\pi^-}$,

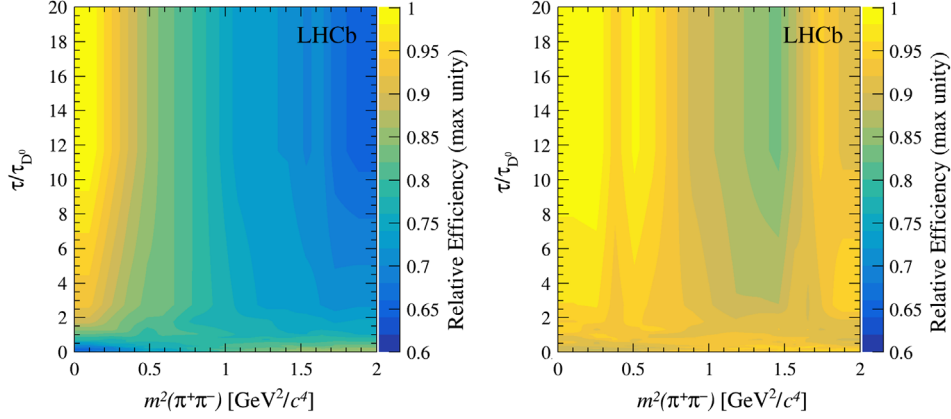


FIG. 3. Relative efficiency as a function of D^0 decay-time and $m^2(\pi^+\pi^-)$ as determined from $\bar{B} \rightarrow D^0(\rightarrow K_S^0\pi^+\pi^-)\mu^-\bar{\nu}_\mu X$ candidates, separately for (left) DD and (right) LL K_S^0 candidates. The distributions are smoothed using bilinear interpolation.

where $\theta_{\pi^+\pi^-}$ is the angle between the direction vector of the $\pi^+\pi^-$ pair in the D^0 meson rest frame and the direction vector of either pion in the $\pi^+\pi^-$ rest frame. Note that each $m^2(\pi^+\pi^-)$ bin comprises events from both sides of the bisector of the Dalitz plot, thus the effect of mixing, which changes the ratios in Eq. (9) as a function of D^0 decay-time, is not present here. The efficiency in this phase space is smoothed and the inverse of the efficiency is assigned as a weight to each signal candidate in data. This efficiency correction suppresses to a large extent the correlation induced from the online selection effects.

A further decorrelation procedure based on data is applied to remove the small remaining correlation. It is determined from the background-subtracted data, once the weights obtained from the simulation have been applied. A decorrelation weight is derived as the inverse of the relative proportion of signal candidates observed in each D^0 decay-time and $m^2(\pi^+\pi^-)$ bin as is done in Fig. 3. In this way, a uniform decay-time acceptance is achieved, without knowledge of the absolute efficiency. Each candidate is thus weighted with the product of the weight from simulation and the data-driven decorrelation weight. From the weighted data sample, yields are extracted for each Dalitz and D^0 decay-time bin, and fitted with the bin-flip method in Sec. VII. The same combined weight is included to generate realistic pseudoexperiments in Sec. VI to validate the method used in this analysis. A similar decorrelation procedure has been used by LHCb in Refs. [9,31].

VI. SYSTEMATIC UNCERTAINTIES

Pseudoexperiments are used to assess the systematic uncertainties and to validate the analysis procedure. The pseudoexperiments are generated by sampling the decay-time-dependent decay rate using the Belle model [33] to describe the amplitudes at $t = 0$. The mixing and CP -violating parameters are included according to the measured values. Phase-space and decay-time acceptance

effects are modeled on simulated samples. The correlation between the D^0 decay-time and the Dalitz plot coordinates is generated using the inverse of the decorrelation weights determined in Sec. V. For each set of pseudoexperiments, these weights are fluctuated within their statistical uncertainties. The pseudoexperiment data can then be processed in exactly the same manner as the collision data. Samples are generated separately for each of the K_S^0 categories, and processed separately up until the last step when all samples are combined to determine the mixing and CP -violating parameters.

To determine the systematic uncertainty due to a given source, pseudodata are generated with the effect in question included. Performing the fit on this dataset determines the bias on the results ensuing from this effect, which however includes statistical effects. This is denoted as the default fit. An additional reference fit is performed where the effect in question is not present or has been corrected for. The difference between the two results represents the systematic uncertainty from the source under consideration.

In Sec. VIA, the reference fit is performed with the pseudodata generated without any detector effects. For determining the rest of the systematic uncertainties, the reconstruction and selection effects are included in the pseudodata in order to represent the data realistically. To avoid double-counting, in these cases the reference fit is the default fit from Sec. VIA.

A. Reconstruction and selection effects

As mentioned above, the reconstruction and selection effects are incorporated into the pseudodata using the acceptance and resolution models obtained from simulation, and the weights from the decorrelation method.

The dominant systematic uncertainties on y_{CP} are due to the neglected decay-time and Dalitz-coordinate resolutions, as well as efficiency variations. Some biases arise in Δx and Δy due to the correlation between resolutions of the Dalitz coordinates, stemming from the K_S^0 mass constraint.

In order to have pseudoexperiments which represent the actual data and to be sure to assess the true effect of the different systematic sources under a realistic setting, these effects are included in all the subsequent studies presented in this section. To avoid double counting of these effects, this baseline bias is included as a systematic uncertainty once, and then the effect of the additional systematic uncertainty sources is calculated with respect to it.

B. Detection asymmetries

The reconstruction efficiency for tracks originating from charged pions varies between the positive and negative charges and depends on momentum. In the $D^0 \rightarrow K_S^0 \pi^+ \pi^-$ decay, this affects the efficiency across the Dalitz plot with respect to its bisector and introduces an artificial flavor asymmetry between the D^0 and \bar{D}^0 mesons. This induces a bias on the measurement of the CP -violating parameters Δx and Δy .

The asymmetry in the $D^0 \rightarrow K_S^0 \pi^+ \pi^-$ sample is estimated using two Cabibbo-favored D_s^+ decays: $D_s^+ \rightarrow \pi^+ \pi^+ \pi^-$ and $D_s^+ \rightarrow \phi(\rightarrow K^+ K^-) \pi^+$. The D_s^+ decay channels are selected with requirements as similar as possible to those for the $D^0 \rightarrow K_S^0 \pi^+ \pi^-$ decays. In the case of the $D_s^+ \rightarrow \pi^+ \pi^+ \pi^-$ decay, the uncorrected, measured asymmetry comprises the asymmetry of a pion pair $\pi^+ \pi^-$, $A_{\text{det}}^{\pi^+ \pi^-}$, the single pion detection asymmetry, $A_{\text{det}}(\pi^+)$, the D_s^+ meson production asymmetry, $A_{\text{prod}}(D_s^+)$, and the asymmetry from the online event selection of the D_s^+ meson, $A_{\text{trig}}(D_s^+)$. Similar components appear for the $D_s^+ \rightarrow \phi(\rightarrow K^+ K^-) \pi^+$ decay, with the exception of the $A_{\text{det}}^{\pi^+ \pi^-}$ component. The asymmetry from $K^+ K^-$ is ignored as $\phi \rightarrow K^+ K^-$ is a self-conjugate decay in which the phase-space of the kaons is identical, thus canceling any reconstruction asymmetry effect. Hence, the asymmetries from these two decays can be expressed to first order as

$$A_{\text{meas}}(D_s^+ \rightarrow \pi^+ \pi^+ \pi^-) = A_{\text{prod}}(D_s^+) + A_{\text{trig}}(D_s^+) + A_{\text{det}}(\pi^+) + A_{\text{det}}^{\pi^+ \pi^-}, \quad (15)$$

$$A_{\text{meas}}(D_s^+ \rightarrow \phi(\rightarrow K^+ K^-) \pi^+) = A_{\text{prod}}(D_s^+) + A_{\text{trig}}(D_s^+) + A_{\text{det}}(\pi^+), \quad (16)$$

where in the $D_s^+ \rightarrow \pi^+ \pi^+ \pi^-$ decay, one of the pion of equal electric charge is paired randomly with the π^- , and the other pion corresponds to the pion in the $D_s^+ \rightarrow \phi(\rightarrow K^+ K^-) \pi^+$ decay. To first approximation, the difference in uncorrected asymmetries between the two D_s^+ decay modes is equal to

$$A_{\text{det}}^{\pi^+ \pi^-} = A_{\text{meas}}(D_s^+ \rightarrow \pi^+ \pi^+ \pi^-) - A_{\text{meas}}(D_s^+ \rightarrow \phi(\rightarrow K^+ K^-) \pi^+). \quad (17)$$

These quantities vary over phase-space and kinematic distributions of the D_s^+ meson. A gradient boosting reweighting algorithm [34] is implemented to equalize the kinematic distributions of the D_s^+ and D^0 meson samples in each bin of $m^2(\pi^+ \pi^-)$, $|\cos \theta_{\pi^+ \pi^-}|$ and D^0 decay-time.

The obtained $A_{\text{det}}^{\pi^+ \pi^-}$ are independent of the Dalitz region and D^0 decay-time. They are found to be -0.017 ± 0.013 and -0.010 ± 0.016 for DD and LL K_S^0 candidates, thus compatible with zero. These values are incorporated in the pseudoexperiment data in addition to the baseline configuration to determine the associated systematic uncertainty.

C. Mass fit model

The bin-flip method deals with ratios of yields between the upper and lower parts of Dalitz plot, which are kinematically similar. The analysis is therefore robust against the choice of a fit model, which will affect the numerator and denominator of the ratios in the same way. However, a possible systematic bias is examined by considering an alternative mass fit model.

The systematic uncertainty from the mass fit is estimated by changing the signal PDF from the Johnson distribution to a crystal ball function [35]. The sensitivity to the choice of the background model is investigated with an alternative polynomial model. The joint alternative fit models are implemented in a fit on the same pseudodata as described in Sec. VI A. The systematic effect in the final measurement is found to be very small, confirming that the measurement is very robust with regard to the choice of the fit models.

D. Unrelated $D^0 \mu^-$ combinations

The data sample has some contamination from $D^0 \mu^-$ combinations in which the muon does not come from the decay of the same b hadron as the D^0 candidate. As the flavor of the D^0 meson is identified from the charge of the accompanying muon, combinations with a random muon have a 50% chance of wrongly tagging the initial flavor of the D^0 meson. Additionally, the decay-time of the D^0 candidate is wrongly estimated, as it is extrapolated to a wrong production vertex.

The probability of wrongly tagging the flavor of a candidate is determined using the $B^- \rightarrow D^0(\rightarrow K^- \pi^+) \times \mu^- X$ decay channel, where it can be estimated by comparing the sign of the kaon and muon after accounting for mixing effects and contributions from doubly Cabibbo-suppressed decays [36]. It is further calibrated using so-called doubly tagged samples of both $D^0 \rightarrow K^- \pi^+$ and signal decays. Doubly tagged events come from a decay chain $\bar{B}^0 \rightarrow D^{*+}(\rightarrow D^0 \pi^+) \mu^- \bar{\nu}_\mu X$, where the flavor of the D^0 can be determined using both the charge of the muon from the semileptonic B meson decay, as well as from the charge of the pion from the D^{*+} meson decay. The decay chain $B^- \rightarrow D^0 \mu^- X$ is henceforth referred to as single-tag.

Once the wrong-tag probability is established, the systematic uncertainty due to unrelated $D^0\mu^-$ combinations is determined through pseudoexperiments.

The $D^0 \rightarrow K^-\pi^+$ samples can be processed with the same requirements as the signal decays, since no variables related to the daughters of the D^0 meson are used in the MVA selection described in Sec. IV. A weighing procedure using a gradient boosting reweighter [34] is implemented to match the kinematics of the $D^0 \rightarrow K^-\pi^+$ samples to that of the $D^0 \rightarrow K_S^0\pi^+\pi^-$ decay. Topological variables related to the B meson decay including the B decay vertex χ^2 , the transverse momenta of the μ and D^0 candidates, and the pseudorapidity of the D^0 meson are used as training variables. The procedure is applied separately for single- and doubly tagged events, as the quantities related to the B decay vertex differ significantly due to the different number of charged tracks used in the reconstruction. The probability of wrongly tagging the $D^0 \rightarrow K^-\pi^+$ decays is determined as

$$\frac{R_{\text{wrong tag}}}{1 + R_{\text{wrong tag}}}, \quad (18)$$

where $R_{\text{wrong tag}}$ is the ratio between yields of the wrong-sign sample and right-sign sample. Wrong and right sign refer to the matching or opposite charges of the muon and kaon for single-tag events, and of the muon and pion from the D^{*+} decay for the doubly tagged events. The yields are extracted from a fit to the D^0 invariant mass distribution. The wrong-tag probability is determined for each decay-time bin separately, but is found to be time-independent and a single value is used for the full sample. The two K_S^0 categories however need to be treated separately, as the dedicated BDTs perform differently.

The wrong-tag probabilities determined for doubly tagged $D^0 \rightarrow K_S^0\pi^+\pi^-$ and $D^0 \rightarrow K^-\pi^+$ decays show good consistency. The difference is quantified as a ratio, which deviates from unity by a few per cent. The ratio is applied as

a scaling factor to the wrong-tag probability obtained from the single-tag $D^0 \rightarrow K^-\pi^+$ sample, to produce the expected wrong-tag probability in the signal channel $\bar{B} \rightarrow D^0(\rightarrow K_S^0\pi^+\pi^-)\mu^-\bar{\nu}_\mu X$: $(0.301 \pm 0.016)\%$ for the DD sample and $(0.125 \pm 0.010)\%$ for the LL sample. The fraction of unrelated $D^0\mu^-$ combinations is twice the measured wrong-tag rate, since such combinations have a 50% probability to be assigned the wrong charge. An ensemble of pseudoexperiments is generated, where for the events representing an unrelated $D^0\mu^-$ combination the sign of the D^0 is flipped with 50% probability, and the D^0 decay-time resolution is smeared to account for the wrong production vertex. The smearing is applied through a Gaussian of width $0.5 \tau_{D^0}$. The systematic uncertainty is obtained by neglecting the generated effect in the analysis of the pseudoexperiment data.

E. Overall systematic uncertainties

A summary of all the uncertainties affecting the measurement is reported in Table I. The statistical uncertainty includes, by construction, also the contribution of the uncertainties on the strong phase inputs. The total systematic uncertainty is the sum in quadrature of the individual components.

To test the robustness of the analysis, several cross-checks are performed. The analysis is repeated in subsets of data, dividing the sample by K_S^0 categories, data-taking periods, magnet polarities, and kinematics of the B meson. Variations of the observables x_{CP} , y_{CP} , Δx , and Δy measured in various subsets of data are all compatible within statistical uncertainties. Results from the bin-flip fit are consistent with the default results when an alternative method is implemented in the decorrelation process [34]. Similar compatibility is observed when the selection process is altered, e.g. a different procedure is used for the multivariate analysis. These cross-checks demonstrate the reliability and robustness of the analysis.

TABLE I. Summary of the uncertainties on the measured quantities. The total systematic uncertainty is the sum in quadrature of the individual components. The uncertainties due to the strong-phase inputs are (by default) included in the statistical uncertainty. Here, to ease comparison with other sources, we also report the separate contributions due to the strong phase inputs and to the statistics of the data sample.

Source	x_{CP} [10^{-3}]	y_{CP} [10^{-3}]	Δx [10^{-3}]	Δy [10^{-3}]
Reconstruction and selection	0.06	0.79	0.28	0.24
Detection asymmetry	0.06	0.03	0.01	0.09
Mass-fit model	0.03	0.09	0.01	0.01
Unrelated $D^0\mu$ combinations	0.24	0.22	0.01	0.05
Total systematic	0.26	0.83	0.28	0.26
Strong phase inputs	0.32	0.68	0.16	0.21
Statistical (w/o phase inputs)	1.45	3.04	0.92	1.91
Statistical	1.48	3.12	0.93	1.92

VII. RESULTS

The mixing and CP -violating parameters are obtained through a fit of the ratios of signal yields observed in regions of the Dalitz plot symmetric about its bisector as a function of decay-time. The signal yields in each Dalitz and decay-time bin are extracted using the PDFs described in Sec. III. The widths of the signal model are fixed from a fit to the whole sample, while the other parameters are left free to vary to account for potential mass shifts between bins due to different resonant contributions. The effect of statistical fluctuations in the low-statistics bins of the upper part of the Dalitz plot is minimized by using the same signal PDF as determined in the fit of the corresponding bin of the higher-yield lower part of the Dalitz plot. External constraints for strong-interaction phases in each bin are used.

The obtained results are

$$\begin{aligned} x_{CP} &= [4.29 \pm 1.48 \pm 0.26] \times 10^{-3}, \\ y_{CP} &= [12.61 \pm 3.12 \pm 0.83] \times 10^{-3}, \\ \Delta x &= [-0.77 \pm 0.93 \pm 0.28] \times 10^{-3}, \\ \Delta y &= [3.01 \pm 1.92 \pm 0.26] \times 10^{-3}, \end{aligned}$$

where the first uncertainty is statistical and includes the contributions due to the uncertainties of the strong phase inputs, and the second is systematic.

Figure 4 shows the CP -averaged yield ratios as well as the difference in yield ratios for D^0 and \bar{D}^0 mesons as a function of decay-time. The fit projections are shown for the nominal fit and a fit where x_{CP} is fixed to zero. The largest sensitivity to x_{CP} is observed, as expected, in the bins 3 and 7 where the strong phase terms, s_3 and s_7 , are closest to unity.

The results are compatible with those measured in the analysis of the $D^{*+} \rightarrow D^0(\rightarrow K_S^0 \pi^+ \pi^-) \pi^+$ decay [9]. No CP violation is observed.

VIII. COMBINATION

As stated in Sec. III, this analysis complements the analogue analysis conducted on $D^{*+} \rightarrow D^0(\rightarrow K_S^0 \pi^+ \pi^-) \pi^+$ decays, dubbed as prompt decays. The two analyses are statistically independent, since the overlap of events is reduced to a negligible level by selection requirements specific to each decay chain. While the semileptonic sample has considerably fewer candidates than the prompt sample, it covers a wider D^0 decay-time: $\tau_{SL}/\tau_{D^0} \in [0, 20]$ while $\tau_{\text{prompt}}/\tau_{D^0} \in [0.3, 8]$. A combination of the two samples is therefore performed.

The systematic uncertainties from most sources can be treated as independent, with the exception of those related to detection asymmetries, as they are estimated using the same control samples. Conservatively, a 100% correlation is assumed for this uncertainty.

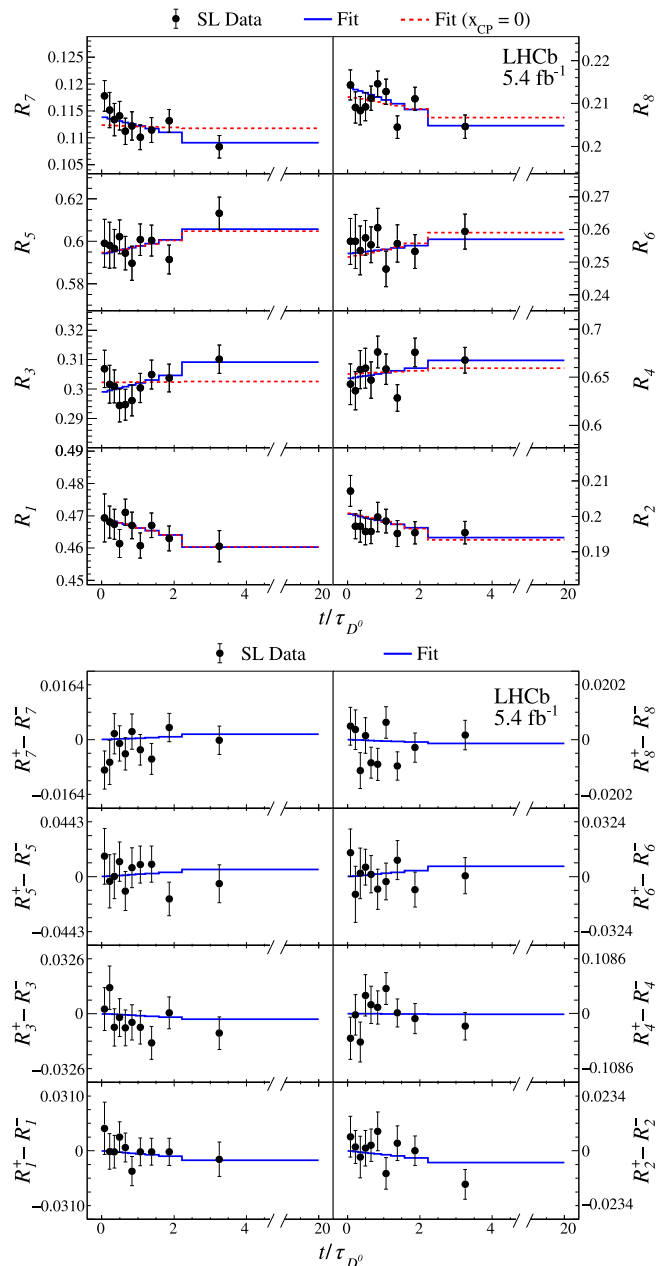


FIG. 4. (Top) CP -averaged yield ratios and (bottom) difference of D^0 and \bar{D}^0 yield ratios as a function of D^0 decay-time for the different Dalitz bins. The solid blue line shows the nominal fit projections and the dashed red line shows the fit projections when x_{CP} is fixed to zero.

The combination method follows the bin-flip analysis of the data sample from the 2011 to 2012 data taking campaign [31]. A simultaneous minimization of a global χ^2 is performed, using the prompt and semileptonic yields of subsamples separated by flavor and other categories (such as K_S^0 type). The parameters r_b , representing the ratio of yields at $t = 0$, are kept separate between the prompt and semileptonic samples as they are affected by different efficiencies in the Dalitz space of the two samples.

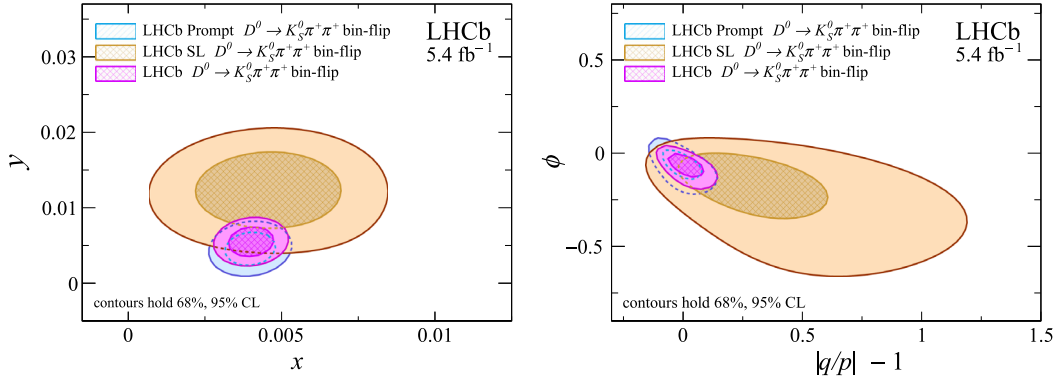


FIG. 5. Two-dimensional 68% and 95% confidence-level contours on (left) (x, y) and (right) $(|q/p| - 1, \phi)$. Results from Run 2 $D^{*+} \rightarrow D^0(\rightarrow K_S^0 \pi^+ \pi^-) \pi^+$ (Prompt) [9], $\bar{B} \rightarrow D^0(\rightarrow K_S^0 \pi^+ \pi^-) \mu^- \bar{\nu}_\mu X$ (SL), and their combination are shown.

Allowing for CP violation, we obtain the following averages:

$$\begin{aligned} x_{CP} &= [4.01 \pm 0.45(\text{stat}) \pm 0.20(\text{syst})] \times 10^{-3}, \\ y_{CP} &= [5.51 \pm 1.16(\text{stat}) \pm 0.59(\text{syst})] \times 10^{-3}, \\ \Delta x &= [-0.29 \pm 0.18(\text{stat}) \pm 0.01(\text{syst})] \times 10^{-3}, \\ \Delta y &= [0.31 \pm 0.35(\text{stat}) \pm 0.13(\text{syst})] \times 10^{-3}. \end{aligned}$$

The value of x_{CP} deviates from zero with a significance of 8.1σ , calculated assuming Gaussian uncertainties. There is no evidence for CP violation.

From the results of the combination fit, x_{CP} , y_{CP} , Δx , and Δy are transformed into x , y , $|q/p|$, and ϕ using Eqs. (3)–(6). A likelihood of these parameters is constructed and confidence intervals are determined from a likelihood-ratio assuming that the measured correlations are independent of the true values of parameters. The PLUGIN method [37] is implemented for the transformation. The method is a generalization of the Feldman and Cousins method [38] and used in the prompt sample [9] as well as the LHCb γ -combination analysis [39]. The results are

$$\begin{aligned} x &= (4.01 \pm 0.49) \times 10^{-3}, \\ y &= (5.5 \pm 1.3) \times 10^{-3}, \\ |q/p| &= 1.012_{-0.048}^{+0.050}, \\ \phi &= -0.061_{-0.044}^{+0.037} \text{ rad.} \end{aligned}$$

IX. SUMMARY

A measurement of charm mixing and CP -violating parameters using $D^0 \rightarrow K_S^0 \pi^+ \pi^-$ decays reconstructed in Run 2 data, with the $\bar{B} \rightarrow D^0(\rightarrow K_S^0 \pi^+ \pi^-) \mu^- \bar{\nu}_\mu X$ semi-leptonic decay used to identify the flavor of the charm meson at production, is presented. The signal yields are extracted from fits to the invariant-mass distributions of the D^0 meson in bins of the Dalitz plot and D^0 decay-time. The

binning of the Dalitz plot is chosen such as to preserve nearly constant values of the strong-interaction phases in each bin, and external constraints for these phases are used. Time-dependent ratios of yields for each pair of Dalitz plot bins symmetric about its bisector are fitted to Eq. (9) to extract the mixing and CP -violating parameters. The results are combined with those from the $D^{*+} \rightarrow D^0(\rightarrow K_S^0 \pi^+ \pi^-) \pi^+$ analysis [9]. Statistical and systematic correlation matrices of the measured variables are presented in the Supplemental Material [40].

Figure 5 shows the measured mixing and CP -violating parameters from the $D^{*+} \rightarrow D^0(\rightarrow K_S^0 \pi^+ \pi^-) \pi^+$ [9] analysis, the $\bar{B} \rightarrow D^0(\rightarrow K_S^0 \pi^+ \pi^-) \mu^- \bar{\nu}_\mu X$ analysis, and their combination. The combination is dominated by the result of the prompt analysis, as expected from the much larger sample size. The results obtained in this analysis are consistent with the results from the prompt analysis and the current world-average values. They represent an independent measurement and complement the knowledge of the charm mixing parameters in an extended region of the D^0 decay-time.

ACKNOWLEDGMENTS

We express our gratitude to our colleagues in the CERN accelerator departments for the excellent performance of the LHC. We thank the technical and administrative staff at the LHCb institutes. We acknowledge support from CERN and from the national agencies: CAPES, CNPq, FAPERJ and FINEP (Brazil); MOST and NSFC (China); CNRS/IN2P3 (France); BMBF, DFG and MPG (Germany); INFN (Italy); NWO (Netherlands); MNiSW and NCN (Poland); MEN/IFA (Romania); MICINN (Spain); SNSF and SER (Switzerland); NASU (Ukraine); STFC (United Kingdom); DOE NP and NSF (USA). We acknowledge the computing resources that are provided by CERN, IN2P3 (France), KIT and DESY (Germany), INFN (Italy), SURF (Netherlands), PIC (Spain), GridPP (United Kingdom), CSCS (Switzerland), IFIN-HH (Romania), CBPF (Brazil),

Polish WLCG (Poland) and NERSC (USA). We are indebted to the communities behind the multiple open-source software packages on which we depend. Individual groups or members have received support from ARC and ARDC (Australia); Minciencias (Colombia); AvH Foundation (Germany); EPLANET, Marie Skłodowska-Curie Actions and ERC (European Union); A*MIDEX, ANR, IPhU and Labex P2IO, and Région Auvergne-

Rhône-Alpes (France); Key Research Program of Frontier Sciences of CAS, CAS PIFI, CAS CCEPP, Fundamental Research Funds for the Central Universities, and Sci. & Tech. Program of Guangzhou (China); GVA, XuntaGal, GENCAT and Prog. Atracción Talento, CM (Spain); SRC (Sweden); the Leverhulme Trust, the Royal Society and UKRI (United Kingdom).

-
- [1] G. Isidori, Y. Nir, and G. Perez, Flavor physics constraints for physics beyond the standard model, *Annu. Rev. Nucl. Part. Sci.* **60**, 355 (2010).
- [2] K. Lande, E. T. Booth, J. Impeduglia, L. M. Lederman, and W. Chinowsky, Observation of long-lived neutral V particles, *Phys. Rev.* **103**, 1901 (1956).
- [3] H. Albrecht *et al.* (ARGUS Collaboration), Observation of $B^0 - \bar{B}^0$ mixing, *Phys. Lett. B* **192**, 245 (1987).
- [4] A. Abulencia *et al.* (CDF Collaboration), Observation of $B_s^0 - \bar{B}_s^0$ Oscillations, *Phys. Rev. Lett.* **97**, 242003 (2006).
- [5] P. A. Zyla *et al.* (Particle Data Group), Review of particle physics, *Prog. Theor. Exp. Phys.* **2020**, 083C01 (2020).
- [6] B. Aubert *et al.* (BABAR Collaboration), Evidence for $D^0 - \bar{D}^0$ Mixing, *Phys. Rev. Lett.* **98**, 211802 (2007).
- [7] M. Starič *et al.* (Belle Collaboration), Evidence for $D^0 - \bar{D}^0$ Mixing, *Phys. Rev. Lett.* **98**, 211803 (2007).
- [8] R. Aaij *et al.* (LHCb Collaboration), Observation of $D^0 - \bar{D}^0$ Oscillations, *Phys. Rev. Lett.* **110**, 101802 (2013).
- [9] R. Aaij *et al.* (LHCb Collaboration), Observation of the Mass Difference Between Neutral Charm-Meson Eigenstates, *Phys. Rev. Lett.* **127**, 111801 (2021).
- [10] R. Aaij *et al.* (LHCb Collaboration), Observation of CP Violation in Charm Decays, *Phys. Rev. Lett.* **122**, 211803 (2019).
- [11] Y. Amhis *et al.* (Heavy Flavor Averaging Group), Averages of b -hadron, c -hadron, and τ -lepton properties as of 2018, *Eur. Phys. J. C* **81**, 226 (2021), updated results and plots available at <https://hflav.web.cern.ch>.
- [12] A. Bondar, A. Poluektov, and V. Vorobiev, Charm mixing in the model-independent analysis of correlated $D^0\bar{D}^0$ decays, *Phys. Rev. D* **82**, 034033 (2010).
- [13] C. Thomas and G. Wilkinson, Model-independent $D^0 - \bar{D}^0$ mixing and CP violation studies with $D^0 \rightarrow K_S^0\pi^+\pi^-$ and $D^0 \rightarrow K_S^0K^+K^-$, *J. High Energy Phys.* **10** (2012) 185.
- [14] A. Di Canto, J. Garra Ticó, T. Gershon, N. Jurik, M. Martinelli, T. Pilař, S. Stahl, and D. Tonelli, Novel method for measuring charm-mixing parameters using multibody decays, *Phys. Rev. D* **99**, 012007 (2019).
- [15] A. A. Alves, Jr. *et al.* (LHCb Collaboration), The LHCb detector at the LHC, *J. Instrum.* **3**, S08005 (2008).
- [16] LHCb Collaboration, LHCb detector performance, *Int. J. Mod. Phys. A* **30**, 1530022 (2015).
- [17] T. Sjöstrand, S. Mrenna, and P. Skands, A brief introduction to PYTHIA 8.1, *Comput. Phys. Commun.* **178**, 852 (2008);
- PYTHIA 6.4 physics and manual, *J. High Energy Phys.* **05** (2006) 026.
- [18] I. Belyaev *et al.*, Handling of the generation of primary events in Gauss, the LHCb simulation framework, *J. Phys. Conf. Ser.* **331**, 032047 (2011).
- [19] D. J. Lange, The EvtGen particle decay simulation package, *Nucl. Instrum. Methods Phys. Res., Sect. A* **462**, 152 (2001).
- [20] N. Davidson, T. Przedzinski, and Z. Was, PHOTOS interface in c++: Technical and physics documentation, *Comput. Phys. Commun.* **199**, 86 (2016).
- [21] J. Allison *et al.* (Geant4 Collaboration), Geant4 developments and applications, *IEEE Trans. Nucl. Sci.* **53**, 270 (2006); S. Agostinelli *et al.* (Geant4 Collaboration), Geant4: A simulation toolkit, *Nucl. Instrum. Methods Phys. Res., Sect. A* **506**, 250 (2003).
- [22] M. Clemencic, G. Corti, S. Easo, C.R. Jones, S. Miglioranza, M. Pappagallo, and P. Robbe, The LHCb simulation application, Gauss: Design, evolution and experience, *J. Phys. Conf. Ser.* **331**, 032023 (2011).
- [23] J. Libby *et al.* (CLEO Collaboration), Model-independent determination of the strong-phase difference between D^0 and $\bar{D}^0 \rightarrow K_{S,L}^0 h^+ h^-$ ($h = \pi, K$) and its impact on the measurement of the CKM angle γ/ϕ_3 , *Phys. Rev. D* **82**, 112006 (2010).
- [24] N. L. Johnson, Systems of frequency curves generated by methods of translation, *Biometrika* **36**, 149 (1949).
- [25] M. Pivk and F. R. Le Diberder, sPlot: A statistical tool to unfold data distributions, *Nucl. Instrum. Methods Phys. Res., Sect. A* **555**, 356 (2005).
- [26] M. Ablikim *et al.* (BESIII Collaboration), Model-independent determination of the relative strong-phase difference between D^0 and $\bar{D}^0 \rightarrow K_{S,L}^0\pi^+\pi^-$ and its impact on the measurement of the CKM angle γ/ϕ_3 , *Phys. Rev. D* **101**, 112002 (2020).
- [27] W. D. Hulsbergen, Decay chain fitting with a Kalman filter, *Nucl. Instrum. Methods Phys. Res., Sect. A* **552**, 566 (2005).
- [28] J. H. Friedman, Greedy function approximation: A gradient boosting machine, *Ann. Stat.* **29**, 1189 (2001).
- [29] J. Stevens and M. Williams, uBoost: A boosting method for producing uniform selection efficiencies from multivariate classifiers, *J. Instrum.* **8**, P12013 (2013).
- [30] A. Blum, A. Kalai, and J. Langford, Beating the hold-out: Bounds for k -fold and progressive cross-validation, in *Proceedings of the Twelfth Annual Conference on*

- Computational Learning Theory, COLT '99* (Association for Computing Machinery, New York, NY, USA, 1999), pp. 203–208.
- [31] R. Aaij *et al.* (LHCb Collaboration), Measurement of the Mass Difference Between Neutral Charm-Meson Eigenstates, *Phys. Rev. Lett.* **122**, 231802 (2019).
- [32] T. Likhomanenko, P. Ilten, E. Khairullin, A. Rogozhnikov, A. Ustyuzhanin, and M. Williams, LHCb topological trigger reoptimization, *J. Phys. Conf. Ser.* **664**, 082025 (2015).
- [33] I. Adachi *et al.* (BABAR and Belle Collaborations), First Evidence for $\cos 2\beta > 0$ and Resolution of the Cabibbo-Kobayashi-Maskawa Quark-Mixing Unitarity Triangle Ambiguity, *Phys. Rev. Lett.* **121**, 261801 (2018).
- [34] A. Rogozhnikov, Reweighting with boosted decision trees, *J. Phys. Conf. Ser.* **762**, 012036 (2016).
- [35] T. Skwarnicki, A study of the radiative CASCADE transitions between the Upsilon-prime and Upsilon resonances, Ph.D. thesis, Institute of Nuclear Physics, Krakow, 1986 [Report No. DESY-F31-86-02].
- [36] R. Aaij *et al.* (LHCb Collaboration), Updated determination of $D^0 - \bar{D}^0$ mixing and CP violation parameters with $D^0 \rightarrow K^+ \pi^-$ decays, *Phys. Rev. D* **97**, 031101 (2018).
- [37] B. Sen, M. Walker, and M. Woodroffe, On the unified method with nuisance parameters, *Stat. Sin.* **19**, 301 (2009).
- [38] G. J. Feldman and R. D. Cousins, A unified approach to the classical statistical analysis of small signals, *Phys. Rev. D* **57**, 3873 (1998).
- [39] R. Aaij *et al.* (LHCb Collaboration), Measurement of the CKM angle γ from a combination of $B^\pm \rightarrow Dh^\pm$ analyses, *Phys. Lett. B* **726**, 151 (2013).
- [40] See Supplemental Material at <http://link.aps.org/supplemental/10.1103/PhysRevD.108.052005> for statistical and systematic correlations between x_{CP} , y_{CP} , Δx , and Δy .

R. Aaij^{1,32}, A. S. W. Abdelmotteleb⁵⁰, C. Abellan Beteta⁴⁴, F. Abudinén⁵⁰, T. Ackernley⁵⁴, B. Adeva⁴⁰, M. Adinolfi⁴⁸, H. Afsharnia⁹, C. Agapopoulou¹³, C. A. Aidala⁷⁷, S. Aiola²⁵, Z. Ajaltouni⁹, S. Akar⁵⁹, K. Akiba³², J. Albrecht¹⁵, F. Alessio⁴², M. Alexander⁵³, A. Alfonso Alberob³⁹, Z. Aliouche⁵⁶, P. Alvarez Cartelle⁴⁹, R. Amalric¹³, S. Amato², J. L. Amey⁴⁸, Y. Amhis^{11,42}, L. An⁴², L. Anderlini²², M. Andersson⁴⁴, A. Andreianov³⁸, M. Andreotti²¹, D. Andreou⁶², D. Ao⁶, F. Archilli¹⁷, A. Artamonov³⁸, M. Artuso⁶², E. Aslanides¹⁰, M. Atzeni⁴⁴, B. Audurier¹², S. Bachmann¹⁷, M. Bachmayer⁴³, J. J. Back⁵⁰, A. Bailly-reyre¹³, P. Baladron Rodriguez⁴⁰, V. Balagura¹², W. Baldini²¹, J. Baptista de Souza Leite¹, M. Barbetti^{22,b}, R. J. Barlow⁵⁶, S. Barsuk¹¹, W. Barter⁵⁵, M. Bartolini⁴⁹, F. Baryshnikov³⁸, J. M. Basels¹⁴, G. Bassi^{29,c}, B. Batsukh⁴, A. Battig¹⁵, A. Bay⁴³, A. Beck⁵⁰, M. Becker¹⁵, F. Bedeschi²⁹, I. B. Bediaga¹, A. Beiter⁶², V. Belavin³⁸, S. Belin⁴⁰, V. Bellee⁴⁴, K. Belous³⁸, I. Belov³⁸, I. Belyaev³⁸, G. Benane¹⁰, G. Bencivenni²³, E. Ben-Haim¹³, A. Berezhnoy³⁸, R. Bernet⁴⁴, S. Bernet Andres⁷⁵, D. Berninghoff¹⁷, H. C. Bernstein⁶², C. Bertella⁵⁶, A. Bertolin²⁸, C. Betancourt⁴⁴, F. Betti⁴², I. A. Bezshyiko⁴⁴, S. Bhasin⁴⁸, J. Bhom³⁵, L. Bian⁶⁸, M. S. Bieker¹⁵, N. V. Biesuz²¹, S. Bifani⁴⁷, P. Billoir¹³, A. Biolchini³², M. Birch⁵⁵, F. C. R. Bishop⁴⁹, A. Bitadze⁵⁶, A. Bizzeti⁵⁶, M. P. Blago⁴⁹, T. Blake⁵⁰, F. Blanc⁴³, S. Blusk⁶², D. Bobulska⁵³, J. A. Boelhauve¹⁵, O. Boente Garcia¹², T. Boettcher⁵⁹, A. Boldyrev³⁸, C. S. Bolognani⁷⁴, R. Bolzonella^{21,d}, N. Bondar^{38,42}, F. Borgato²⁸, S. Borghi⁵⁶, M. Borsato¹⁷, J. T. Borsuk³⁵, S. A. Bouchiba⁴³, T. J. V. Bowcock⁵⁴, A. Boyer⁴², C. Bozzi²¹, M. J. Bradley⁵⁵, S. Braun⁶⁰, A. Brea Rodriguez⁴⁰, J. Brodzicka³⁵, A. Brossa Gonzalo⁴⁰, J. Brown⁵⁴, D. Brundu²⁷, A. Buonauro⁴⁴, L. Buonincontri²⁸, A. T. Burke⁵⁶, C. Burr⁴², A. Bursche⁶⁶, A. Butkevich³⁸, J. S. Butter³², J. Buytaert⁴², W. Byczynski⁴², S. Cadeddu²⁷, H. Cai⁶⁸, R. Calabrese^{21,d}, L. Calefice¹⁵, S. Cali²³, R. Calladine⁴⁷, M. Calvi^{26,e}, M. Calvo Gomez⁷⁵, P. Campana²³, D. H. Campora Perez⁷⁴, A. F. Campoverde Quezada⁶, S. Capelli^{26,e}, L. Capriotti^{20,f}, A. Carbone^{20,f}, G. Carboni³¹, R. Cardinale^{24,g}, A. Cardini²⁷, I. Carli⁴, P. Carniti^{26,e}, L. Carus¹⁴, A. Casais Vidal⁴⁰, R. Caspary¹⁷, G. Casse⁵⁴, M. Cattaneo⁴², G. Cavallero⁴², V. Cavallini^{21,d}, S. Celani⁴³, J. Cerasoli¹⁰, D. Cervenkov⁵⁷, A. J. Chadwick⁵⁴, M. G. Chapman⁴⁸, M. Charles¹³, Ph. Charpentier⁴², C. A. Chavez Barajas⁵⁴, M. Chefdeville⁸, C. Chen³, S. Chen⁴, A. Chernov³⁵, S. Chernyshenko⁴⁶, V. Chobanova⁴⁰, S. Cholak⁴³, M. Chruszcz³⁵, A. Chubykin³⁸, V. Chulikov³⁸, P. Ciambone²³, M. F. Cicala⁵⁰, X. Cid Vidal⁴⁰, G. Ciezarek⁴², G. Ciullo^{21,d}, P. E. L. Clarke⁵², M. Clemencic⁴², H. V. Cliff⁴⁹, J. Closier⁴², J. L. Cobbledick⁵⁶, V. Coco⁴², J. A. B. Coelho¹¹, J. Cogan¹⁰, E. Cogneras⁹, L. Cojocariu³⁷, P. Collins⁴², T. Colombo⁴², L. Congedo¹⁹, A. Contu²⁷, N. Cooke⁴⁷, I. Corredoira⁴⁰, G. Corti⁴², B. Couturier⁴², D. C. Craik⁵⁸, J. Crkovačka⁶¹, M. Cruz Torres^{1,h}, R. Currie⁵², C. L. Da Silva⁶¹, S. Dadabaev³⁸, L. Dai⁶⁵, X. Dai⁵, E. Dall’Oco¹⁵, J. Dalseno⁴⁰, C. D’Ambrosio⁴², J. Daniel⁹, A. Danilina³⁸, P. d’Argent¹⁵, J. E. Davies⁵⁶, A. Davis⁵⁶, O. De Aguiar Francisco⁵⁶, J. de Boer⁴², K. De Bruyn⁷³, S. De Capua⁵⁶, M. De Cian⁴³, U. De Freitas Carneiro Da Graca¹, E. De Lucia²³, J. M. De Miranda¹, L. De Paula², M. De Serio^{19,i}

D. De Simone⁴⁴, P. De Simone²³, F. De Vellis¹⁵, J. A. de Vries⁷⁴, C. T. Dean⁶¹, F. Debernardis^{19,i}, D. Decamp⁸, V. Dedu¹⁰, L. Del Buono¹³, B. Delaney⁵⁸, H.-P. Dembinski¹⁵, V. Denysenko⁴⁴, O. Deschamps⁹, F. Dettori^{27,j}, B. Dey⁷¹, A. Di Canto⁴², A. Di Cicco²³, P. Di Nezza²³, I. Diachkov³⁸, S. Didenko³⁸, L. Dieste Maronas⁴⁰, S. Ding⁶², V. Dobishuk⁴⁶, A. Dolmatov³⁸, C. Dong³, A. M. Donohoe¹⁸, F. Dordei²⁷, A. C. dos Reis¹, L. Douglas⁵³, A. G. Downes⁸, M. W. Dudek³⁵, L. Dufour⁴², V. Duk⁷², P. Durante⁴², J. M. Durham⁶¹, D. Dutta⁵⁶, A. Dziurda³⁵, A. Dzyuba³⁸, S. Easo⁵¹, U. Egede⁶³, V. Egorychev³⁸, S. Eidelman^{38,a}, C. Eirea Orro⁴⁰, S. Eisenhardt⁵², E. Ejopu⁵⁶, S. Ek-In⁴³, L. Eklund⁷⁶, S. Ely⁶², A. Ene³⁷, E. Epple⁶¹, S. Escher¹⁴, J. Eschle⁴⁴, S. Esen⁴⁴, T. Evans⁵⁶, F. Fabiano^{27,j}, L. N. Falcao¹, Y. Fan⁶, B. Fang⁶⁸, S. Farry⁵⁴, D. Fazzini^{26,e}, M. Feo⁴², M. Fernandez Gomez⁴⁰, A. D. Fernandez⁶⁰, F. Ferrari²⁰, L. Ferreira Lopes⁴³, F. Ferreira Rodrigues², S. Ferreres Sole³², M. Ferrillo⁴⁴, M. Ferro-Luzzi⁴², S. Filippov³⁸, R. A. Fini¹⁹, M. Fiorini^{21,d}, M. Firlej³⁴, K. M. Fischer⁵⁷, D. S. Fitzgerald⁷⁷, C. Fitzpatrick⁵⁶, T. Fiutowski³⁴, F. Fleuret¹², M. Fontana¹³, F. Fontanelli^{24,g}, R. Forty⁴², D. Foulds-Holt⁴⁹, V. Franco Lima⁵⁴, M. Franco Sevilla⁶⁰, M. Frank⁴², E. Franzoso^{21,d}, G. Frau¹⁷, C. Frei⁴², D. A. Friday⁵³, J. Fu⁶, Q. Fuehring¹⁵, T. Fulghesu¹³, E. Gabriel³², G. Galati^{19,i}, M. D. Galati⁷³, A. Gallas Torreira⁴⁰, D. Galli^{20,f}, S. Gambetta^{52,42}, Y. Gan³, M. Gandelman², P. Gandini²⁵, Y. Gao⁵, M. Garau^{27,j}, L. M. Garcia Martin⁵⁰, P. Garcia Moreno³⁹, J. Garcia Pardiñas^{26,e}, B. Garcia Plana⁴⁰, F. A. Garcia Rosales¹², L. Garrido³⁹, C. Gaspar⁴², R. E. Geertsema³², D. Gerick¹⁷, L. L. Gerken¹⁵, E. Gersabeck⁵⁶, M. Gersabeck⁵⁶, T. Gershon⁵⁰, L. Giambastiani²⁸, V. Gibson⁴⁹, H. K. Giemza³⁶, A. L. Gilman⁵⁷, M. Giovannetti^{23,k}, A. Gioventù⁴⁰, P. Gironella Gironell³⁹, C. Giugliano^{21,d}, M. A. Giza³⁵, K. Gizdov⁵², E. L. Gkougkousis⁴², V. V. Gligorov^{13,42}, C. Göbel⁶⁴, E. Golobardes⁷⁵, D. Golubkov³⁸, A. Golutvin^{55,38}, A. Gomes^{1,l}, S. Gomez Fernandez³⁹, F. Goncalves Abrantes⁵⁷, M. Goncerz³⁵, G. Gong³, I. V. Gorelov³⁸, C. Gotti²⁶, J. P. Grabowski¹⁷, T. Grammatico¹³, L. A. Granado Cardoso⁴², E. Graugés³⁹, E. Graverini⁴³, G. Graziani¹, A. T. Grecu³⁷, L. M. Greeven³², N. A. Grieser⁴, L. Grillo⁵³, S. Gromov³⁸, B. R. Gruberg Cazon⁵⁷, C. Gu³, M. Guarise^{21,d}, M. Guittiere¹¹, P. A. Günther¹⁷, E. Gushchin³⁸, A. Guth¹⁴, Y. Guz³⁸, T. Gys⁴², T. Hadavizadeh⁶³, G. Haefeli⁴³, C. Haen⁴², J. Haimberger⁴², S. C. Haines⁴⁹, T. Halewood-leagas⁵⁴, M. M. Halvorsen⁴², P. M. Hamilton⁶⁰, J. Hammerich⁵⁴, Q. Han⁷, X. Han¹⁷, E. B. Hansen⁵⁶, S. Hansmann-Menzemer^{17,42}, L. Hao⁶, N. Harnew⁵⁷, T. Harrison⁵⁴, C. Hasse⁴², M. Hatch⁴², J. He^{6,m}, K. Heijhoff³², K. Heinicke¹⁵, C. Henderson⁵⁹, R. D. L. Henderson^{63,50}, A. M. Hennequin⁵⁸, K. Hennessy⁵⁴, L. Henry⁴², J. Herd⁵⁵, J. Heuel¹⁴, A. Hicheur², D. Hill⁴³, M. Hilton⁵⁶, S. E. Hollitt¹⁵, J. Horswill⁵⁶, R. Hou⁷, Y. Hou⁸, J. Hu¹⁷, J. Hu⁶⁶, W. Hu⁵, X. Hu³, W. Huang⁶, X. Huang⁶⁸, W. Hulsbergen³², R. J. Hunter⁵⁰, M. Hushchyn³⁸, D. Hutchcroft⁵⁴, P. Ibis¹⁵, M. Idzik³⁴, D. Ilin³⁸, P. Ilten⁵⁹, A. Inglessi³⁸, A. Iniukhin³⁸, A. Ishteev³⁸, K. Ivshin³⁸, R. Jacobsson⁴², H. Jage¹⁴, S. J. Jaimes Elles⁴¹, S. Jakobsen⁴², E. Jans³², B. K. Jashal⁴¹, A. Jawahery⁶⁰, V. Jevtic¹⁵, E. Jiang⁶⁰, X. Jiang^{4,6}, Y. Jiang⁶, M. John⁵⁷, D. Johnson⁵⁸, C. R. Jones⁴⁹, T. P. Jones⁵⁰, B. Jost⁴², N. Jurik⁴², I. Juszczak³⁵, S. Kandybei⁴⁵, Y. Kang³, M. Karacson⁴², D. Karpenkov³⁸, M. Karpov³⁸, J. W. Kautz⁵⁹, F. Keizer⁴², D. M. Keller⁶², M. Kenzie⁵⁰, T. Ketel³², B. Khanji¹⁵, A. Kharisova³⁸, S. Kholodenko³⁸, G. Khreich¹¹, T. Kim¹⁴, V. S. Kirsebom⁴³, O. Kitouni⁵⁸, S. Klaver³³, N. Kleijne^{29,c}, K. Klimaszewski³⁶, M. R. Kmiec³⁶, S. Koliiev⁴⁶, A. Kondybayeva³⁸, A. Konoplyannikov³⁸, P. Kopciewicz³⁴, R. Kopečna¹⁷, P. Koppenburg³², M. Korolev³⁸, I. Kostiuik^{32,46}, O. Kot⁴⁶, S. Kotriakhova¹, A. Kozachuk³⁸, P. Kravchenko³⁸, L. Kravchuk³⁸, R. D. Krawczyk⁴², M. Kreps⁵⁰, S. Kretzschmar¹⁴, P. Krokovny³⁸, W. Krupa³⁴, W. Krzemien³⁶, J. Kubat¹⁷, W. Kucewicz^{35,34}, M. Kucharczyk³⁵, V. Kudryavtsev³⁸, G. J. Kunde⁶¹, A. Kupsc⁷⁶, D. Lacarrere⁴², G. Lafferty⁵⁶, A. Lai²⁷, A. Lampis^{27,j}, D. Lancierini⁴⁴, C. Landesa Gomez⁴⁰, J. J. Lane⁵⁶, R. Lane⁴⁸, G. Lanfranchi²³, C. Langenbruch¹⁴, J. Langer¹⁵, O. Lantwin³⁸, T. Latham⁵⁰, F. Lazzari^{29,n}, M. Lazzaroni^{25,o}, R. Le Gac¹⁰, S. H. Lee⁷⁷, R. Lefèvre⁹, A. Leflat³⁸, S. Legotin³⁸, P. Lenisa^{21,d}, O. Leroy¹⁰, T. Lesiak³⁵, B. Leverington¹⁷, A. Li³, H. Li⁶⁶, K. Li⁷, P. Li¹⁷, P.-R. Li⁶⁷, S. Li⁷, T. Li⁶⁶, Y. Li⁴, Z. Li⁶², X. Liang⁶², C. Lin⁶, T. Lin⁵¹, R. Lindner⁴², V. Lisovskyi¹⁵, R. Litvinov^{27,j}, G. Liu⁶⁶, H. Liu⁶, Q. Liu⁶, S. Liu^{4,6}, A. Lobo Salvia³⁹, A. Loi²⁷, R. Lollini⁷², J. Lomba Castro⁴⁰, I. Longstaff⁵³, J. H. Lopes², A. Lopez Huertas³⁹, S. López Soliño⁴⁰, G. H. Lovell⁴⁹, Y. Lu^{4,p}, C. Lucarelli^{22,b}, D. Lucchesi^{28,q}, S. Luchuk³⁸, M. Lucio Martinez⁷⁴, V. Lukashenko^{32,46}, Y. Luo³, A. Lupato⁵⁶, E. Luppi^{21,d}, A. Lusiani^{29,c}, K. Lynch¹⁸, X.-R. Lyu⁶, L. Ma⁴, R. Ma⁶, S. Maccolini²⁰, F. Machefert¹¹, F. Maciuc³⁷, I. Mackay⁵⁷, V. Macko⁴³, P. Mackowiak¹⁵, L. R. Madhan Mohan⁴⁸, A. Maevskiy³⁸

D. Maisuzenko³⁸, M. W. Majewski³⁴, J. J. Malczewski³⁵, S. Malde⁵⁷, B. Malecki^{35,42}, A. Malinin³⁸, T. Maltsev³⁸,
 G. Manca^{27,j}, G. Mancinelli¹⁰, C. Mancuso^{11,25,o}, D. Manuzzi²⁰, C. A. Manzari⁴⁴, D. Marangotto^{25,o},
 J. F. Marchand⁸, U. Marconi²⁰, S. Mariani^{22,b}, C. Marin Benito³⁹, J. Marks¹⁷, A. M. Marshall⁴⁸, P. J. Marshall⁵⁴,
 G. Martelli^{72,r}, G. Martellotti³⁰, L. Martinazzoli^{42,e}, M. Martinelli^{26,e}, D. Martinez Santos⁴⁰, F. Martinez Vidal⁴¹,
 A. Massafferri¹, M. Materok¹⁴, R. Matev⁴², A. Mathad⁴⁴, V. Matiunin³⁸, C. Matteuzzi²⁶, K. R. Mattioli⁷⁷,
 A. Mauri³², E. Maurice¹², J. Mauricio³⁹, M. Mazurek⁴², M. McCann⁵⁵, L. McConnell¹⁸, T. H. McGrath⁵⁶,
 N. T. McHugh⁵³, A. McNab⁵⁶, R. McNulty¹⁸, J. V. Mead⁵⁴, B. Meadows⁵⁹, G. Meier¹⁵, D. Melnychuk³⁶,
 S. Meloni^{26,e}, M. Merk^{32,74}, A. Merli^{25,o}, L. Meyer Garcia², D. Miao^{4,6}, M. Mikhasenko^{70,s}, D. A. Milanese⁶⁹,
 E. Millard⁵⁰, M. Milovanovic⁴², M.-N. Minard^{8,a}, A. Minotti^{26,e}, T. Miralles⁹, S. E. Mitchell⁵², B. Mitreska⁵⁶,
 D. S. Mitzel¹⁵, A. Mödden¹⁵, R. A. Mohammed⁵⁷, R. D. Moise¹⁴, S. Mokhnenko³⁸, T. Mombächer⁴⁰,
 M. Monk^{50,63}, I. A. Monroy⁶⁹, S. Monteil⁹, M. Morandin²⁸, G. Morello²³, M. J. Morello^{29,c}, J. Moron³⁴,
 A. B. Morris⁷⁰, A. G. Morris⁵⁰, R. Mountain⁶², H. Mu³, E. Muhammad⁵⁰, F. Muheim⁵², M. Mulder⁷³,
 K. Müller⁴⁴, C. H. Murphy⁵⁷, D. Murray⁵⁶, R. Murta⁵⁵, P. Muzzetto^{27,j}, P. Naik⁴⁸, T. Nakada⁴³,
 R. Nandakumar⁵¹, T. Nanut⁴², I. Nasteva², M. Needham⁵², N. Neri^{25,o}, S. Neubert⁷⁰, N. Neufeld⁴²,
 P. Neustroev³⁸, R. Newcombe⁵⁵, J. Nicolini^{15,11}, E. M. Niel⁴³, S. Nieswand¹⁴, N. Nikitin³⁸, N. S. Nolte⁵⁸,
 C. Normand^{8,27,j}, J. Novoa Fernandez⁴⁰, C. Nunez⁷⁷, A. Oblakowska-Mucha³⁴, V. Obraztsov³⁸, T. Oeser¹⁴,
 D. P. O’Hanlon⁴⁸, S. Okamura^{21,d}, R. Oldeman^{27,j}, F. Oliva⁵², M. E. Olivares⁶², C. J. G. Onderwater⁷³,
 R. H. O’Neil⁵², J. M. Otalora Goicochea², T. Ovsianikova³⁸, P. Owen⁴⁴, A. Oyanguren⁴¹, O. Ozelcik⁵²,
 K. O. Padeken⁷⁰, B. Pagare⁵⁰, P. R. Pais⁴², T. Pajero⁵⁷, A. Palano¹⁹, M. Palutan²³, Y. Pan⁵⁶, G. Panshin³⁸,
 L. Paolucci⁵⁰, A. Papanestis⁵¹, M. Pappagallo^{19,i}, L. L. Pappalardo^{21,d}, C. Pappenheimer⁵⁹, W. Parker⁶⁰,
 C. Parkes⁵⁶, B. Passalacqua^{21,d}, G. Passaleva²², A. Pastore¹⁹, M. Patel⁵⁵, C. Patrignani^{20,f}, C. J. Pawley⁷⁴,
 A. Pearce⁴², A. Pellegrino³², M. Pepe Altarelli⁴², S. Perazzini²⁰, D. Pereima³⁸, A. Pereiro Castro⁴⁰, P. Perret⁹,
 M. Petric⁵³, K. Petridis⁴⁸, A. Petrolini^{24,g}, A. Petrov³⁸, S. Petrucci⁵², M. Petruzzo²⁵, H. Pham⁶², A. Philippov³⁸,
 R. Piandani⁶, L. Pica^{29,c}, M. Piccini⁷², B. Pietrzyk⁸, G. Pietrzyk¹¹, M. Pili⁵⁷, D. Pinci³⁰, F. Pisani⁴²,
 M. Pizzichemi^{26,42,e}, V. Placinta³⁷, J. Plews⁴⁷, M. Plo Casasus⁴⁰, F. Polci^{13,42}, M. Poli Lener²³, M. Poliakov⁶²,
 A. Poluektov¹⁰, N. Polukhina³⁸, I. Polyakov⁴², E. Polycarpo², S. Ponce⁴², D. Popov^{6,42}, S. Popov³⁸,
 S. Poslavskii³⁸, K. Prasanth³⁵, L. Promberger⁴², C. Prouve⁴⁰, V. Pugatch⁴⁶, V. Puill¹¹, G. Punzi^{29,t}, H. R. Qi³,
 W. Qian⁶, N. Qin³, S. Qu³, R. Quagliani⁴³, N. V. Raab¹⁸, R. I. Rabadan Trejo⁶, B. Rachwal³⁴,
 J. H. Rademacker⁴⁸, R. Rajagopalan⁶², M. Rama²⁹, M. Ramos Pernas⁵⁰, M. S. Rangel², F. Ratnikov³⁸,
 G. Raven^{33,42}, M. Rebollo De Miguel⁴¹, F. Redi⁴², J. Reich⁴⁸, F. Reiss⁵⁶, C. Remon Alepuz⁴¹, Z. Ren³,
 V. Renaudin⁵⁷, P. K. Resmi¹⁰, R. Ribatti^{29,c}, A. M. Ricci²⁷, S. Ricciardi⁵¹, K. Richardson⁵⁸,
 M. Richardson-Slipper⁵², K. Rinnert⁵⁴, P. Robbe¹¹, G. Robertson⁵², A. B. Rodrigues⁴³, E. Rodrigues⁵⁴,
 E. Rodriguez Fernandez⁴⁰, J. A. Rodriguez Lopez⁶⁹, E. Rodriguez Rodriguez⁴⁰, A. Rollings⁵⁷, P. Roloff⁴²,
 V. Romanovskiy³⁸, M. Romero Lamas⁴⁰, A. Romero Vidal⁴⁰, J. D. Roth^{77,a}, M. Rotondo²³, M. S. Rudolph⁶²,
 T. Ruf⁴², R. A. Ruiz Fernandez⁴⁰, J. Ruiz Vidal⁴¹, A. Ryzhikov³⁸, J. Ryzka³⁴, J. J. Saborido Silva⁴⁰,
 N. Sagidova³⁸, N. Sahoo⁴⁷, B. Saitta^{27,j}, M. Salomoni⁴², C. Sanchez Gras³², I. Sanderswood⁴¹,
 R. Santacesaria³⁰, C. Santamarina Rios⁴⁰, M. Santimaria²³, E. Santovetti^{31,k}, D. Saranin³⁸, G. Sarpis¹⁴,
 M. Sarpis⁷⁰, A. Sarti³⁰, C. Satriano^{30,u}, A. Satta³¹, M. Saur¹⁵, D. Savrina³⁸, H. Sazak⁹,
 L. G. Scantlebury Smead⁵⁷, A. Scarabotto¹³, S. Schael¹⁴, S. Scherl⁵⁴, M. Schiller⁵³, H. Schindler⁴²,
 M. Schmelling¹⁶, B. Schmidt⁴², S. Schmitt¹⁴, O. Schneider⁴³, A. Schopper⁴², M. Schubiger³², S. Schulte⁴³,
 M. H. Schune¹¹, R. Schwemmer⁴², B. Sciascia^{23,42}, A. Sciucati⁴², S. Sellam⁴⁰, A. Semennikov³⁸,
 M. Senghi Soares³³, A. Sergi^{24,g}, N. Serra⁴⁴, L. Sestini²⁸, A. Seuthe¹⁵, Y. Shang⁵, D. M. Shangase⁷⁷,
 M. Shapkin³⁸, I. Shchemerov³⁸, L. Shchutska⁴³, T. Shears⁵⁴, L. Shekhtman³⁸, Z. Shen⁵, S. Sheng^{4,6},
 V. Shevchenko³⁸, B. Shi⁶, E. B. Shields^{26,e}, Y. Shimizu¹¹, E. Shmanin³⁸, J. D. Shupperd⁶², B. G. Siddi^{21,d},
 R. Silva Coutinho⁴⁴, G. Simi²⁸, S. Simone^{19,i}, M. Singla⁶³, N. Skidmore⁵⁶, R. Skuza¹⁷, T. Skwarnicki⁶²,
 M. W. Slater⁴⁷, J. C. Smallwood⁵⁷, J. G. Smeaton⁴⁹, E. Smith⁴⁴, K. Smith⁶¹, M. Smith⁵⁵, A. Snoch³²,
 L. Soares Lavoura⁹, M. D. Sokoloff⁵⁹, F. J. P. Soler⁵³, A. Solomin^{38,48}, A. Solovev³⁸, I. Solovyevev³⁸, R. Song⁶³,
 F. L. Souza De Almeida², B. Souza De Paula², B. Spaan^{15,a}, E. Spadaro Norella^{25,o}, E. Spiridenkov³⁸, P. Spradlin⁵³,
 V. Sriskaran⁴², F. Stagni⁴², M. Stahl⁵⁹, S. Stahl⁴², S. Stanislaus⁵⁷, E. N. Stein⁴², O. Steinkamp⁴⁴, O. Stenyakin³⁸,

H. Stevens¹⁵, S. Stone^{62,a}, D. Strelakina³⁸, F. Suljik⁵⁷, J. Sun²⁷, L. Sun⁶⁸, Y. Sun⁶⁰, P. Svihra⁵⁶, P. N. Swallow⁴⁷, K. Swientek³⁴, A. Szabelski³⁶, T. Szumlak³⁴, M. Szymanski⁴², Y. Tan³, S. Taneja⁵⁶, A. R. Tanner⁴⁸, M. D. Tat⁵⁷, A. Terentev³⁸, F. Teubert⁴², E. Thomas⁴², D. J. D. Thompson⁴⁷, K. A. Thomson⁵⁴, H. Tilquin⁵⁵, V. Tisserand⁹, S. T'Jampens⁸, M. Tobin⁴, L. Tomassetti^{21,d}, G. Tonani^{25,o}, X. Tong⁵, D. Torres Machado¹, D. Y. Tou³, E. Trifonova³⁸, S. M. Trilov⁴⁸, C. Trippel⁴³, G. Tuci⁶, A. Tully⁴³, N. Tuning³², A. Ukleja³⁶, D. J. Unverzagt¹⁷, E. Ursov³⁸, A. Usachov³², A. Ustyuzhanin³⁸, U. Uwer¹⁷, A. Vagner³⁸, V. Vagnoni²⁰, A. Valassi⁴², G. Valenti²⁰, N. Valls Canudas⁷⁵, M. van Beuzekom³², M. Van Dijk⁴³, H. Van Hecke⁶¹, E. van Herwijnen³⁸, C. B. Van Hulse^{40,v}, M. van Veghel⁷³, R. Vazquez Gomez³⁹, P. Vazquez Regueiro⁴⁰, C. Vázquez Sierra⁴², S. Vecchi²¹, J. J. Velthuis⁴⁸, M. Veltri^{22,w}, A. Venkateswaran⁴³, M. Veronesi³², M. Vesterinen⁵⁰, D. Vieira⁵⁹, M. Vieites Diaz⁴³, X. Vilasis-Cardona⁷⁵, E. Vilella Figueras⁵⁴, A. Villa²⁰, P. Vincent¹³, F. C. Volle¹¹, D. vom Bruch¹⁰, A. Vorobyev³⁸, V. Vorobyev³⁸, N. Voropaev³⁸, K. Vos⁷⁴, C. Vrahas⁵², R. Waldi¹⁷, J. Walsh²⁹, G. Wan⁵, C. Wang¹⁷, J. Wang⁵, J. Wang⁴, J. Wang³, J. Wang⁶⁸, M. Wang⁵, R. Wang⁴⁸, X. Wang⁶⁶, Y. Wang⁷, Z. Wang⁴⁴, Z. Wang³, Z. Wang⁶, J. A. Ward^{50,63}, N. K. Watson⁴⁷, D. Websdale⁵⁵, Y. Wei⁵, C. Weissler⁵⁸, B. D. C. Westhenry⁴⁸, D. J. White⁵⁶, M. Whitehead⁵³, A. R. Wiederhold⁵⁰, D. Wiedner¹⁵, G. Wilkinson⁵⁷, M. K. Wilkinson⁵⁹, I. Williams⁴⁹, M. Williams⁵⁸, M. R. J. Williams⁵², R. Williams⁴⁹, F. F. Wilson⁵¹, W. Wislicki³⁶, M. Witek³⁵, L. Witola¹⁷, C. P. Wong⁶¹, G. Wormser¹¹, S. A. Wotton⁴⁹, H. Wu⁶², K. Wyllie⁴², Z. Xiang⁶, D. Xiao⁷, Y. Xie⁷, A. Xu⁵, J. Xu⁶, L. Xu³, L. Xu³, M. Xu⁵⁰, Q. Xu⁶, Z. Xu⁹, Z. Xu⁶, D. Yang³, S. Yang⁶, Y. Yang⁶, Z. Yang⁵, Z. Yang⁶⁰, L. E. Yeomans⁵⁴, V. Yeroshenko¹¹, H. Yeung⁵⁶, H. Yin⁷, J. Yu⁶⁵, X. Yuan⁶², E. Zaffaroni⁴³, M. Zavertyaev¹⁶, M. Zdybal³⁵, O. Zenaiev⁴², M. Zeng³, C. Zhang⁵, D. Zhang⁷, L. Zhang³, S. Zhang⁶⁵, S. Zhang⁵, Y. Zhang⁵, Y. Zhang⁵⁷, A. Zharkova³⁸, A. Zhelezov¹⁷, Y. Zheng⁶, T. Zhou⁵, X. Zhou⁶, Y. Zhou⁶, V. Zhovkovska¹¹, X. Zhu³, X. Zhu⁷, Z. Zhu⁶, V. Zhukov^{14,38}, Q. Zou^{4,6}, S. Zucchelli^{20,f}, D. Zuliani²⁸ and G. Zunica⁵⁶

(LHCb Collaboration)

¹*Centro Brasileiro de Pesquisas Físicas (CBPF), Rio de Janeiro, Brazil*

²*Universidade Federal do Rio de Janeiro (UFRJ), Rio de Janeiro, Brazil*

³*Center for High Energy Physics, Tsinghua University, Beijing, China*

⁴*Institute Of High Energy Physics (IHEP), Beijing, China*

⁵*School of Physics State Key Laboratory of Nuclear Physics and Technology, Peking University, Beijing, China*

⁶*University of Chinese Academy of Sciences, Beijing, China*

⁷*Institute of Particle Physics, Central China Normal University, Wuhan, Hubei, China*

⁸*Université Savoie Mont Blanc, CNRS, IN2P3-LAPP, Annecy, France*

⁹*Université Clermont Auvergne, CNRS/IN2P3, LPC, Clermont-Ferrand, France*

¹⁰*Aix Marseille Université, CNRS/IN2P3, CPPM, Marseille, France*

¹¹*Université Paris-Saclay, CNRS/IN2P3, IJCLab, Orsay, France*

¹²*Laboratoire Leprince-Ringuet, CNRS/IN2P3, Ecole Polytechnique, Institut Polytechnique de Paris, Palaiseau, France*

¹³*LPNHE, Sorbonne Université, Paris Diderot Sorbonne Paris Cité, CNRS/IN2P3, Paris, France*

¹⁴*I. Physikalisches Institut, RWTH Aachen University, Aachen, Germany*

¹⁵*Fakultät Physik, Technische Universität Dortmund, Dortmund, Germany*

¹⁶*Max-Planck-Institut für Kernphysik (MPIK), Heidelberg, Germany*

¹⁷*Physikalisches Institut, Ruprecht-Karls-Universität Heidelberg, Heidelberg, Germany*

¹⁸*School of Physics, University College Dublin, Dublin, Ireland*

¹⁹*INFN Sezione di Bari, Bari, Italy*

²⁰*INFN Sezione di Bologna, Bologna, Italy*

²¹*INFN Sezione di Ferrara, Ferrara, Italy*

²²*INFN Sezione di Firenze, Firenze, Italy*

²³*INFN Laboratori Nazionali di Frascati, Frascati, Italy*

²⁴*INFN Sezione di Genova, Genova, Italy*

²⁵*INFN Sezione di Milano, Milano, Italy*

²⁶*INFN Sezione di Milano-Bicocca, Milano, Italy*

²⁷*INFN Sezione di Cagliari, Monserrato, Italy*

²⁸*Università degli Studi di Padova, Università e INFN, Padova, Italy*

- ²⁹*INFN Sezione di Pisa, Pisa, Italy*
- ³⁰*INFN Sezione di Roma La Sapienza, Roma, Italy*
- ³¹*INFN Sezione di Roma Tor Vergata, Roma, Italy*
- ³²*Nikhef National Institute for Subatomic Physics, Amsterdam, Netherlands*
- ³³*Nikhef National Institute for Subatomic Physics and VU University Amsterdam, Amsterdam, Netherlands*
- ³⁴*AGH—University of Science and Technology, Faculty of Physics and Applied Computer Science, Kraków, Poland*
- ³⁵*Henryk Niewodniczanski Institute of Nuclear Physics Polish Academy of Sciences, Kraków, Poland*
- ³⁶*National Center for Nuclear Research (NCBJ), Warsaw, Poland*
- ³⁷*Horia Hulubei National Institute of Physics and Nuclear Engineering, Bucharest-Magurele, Romania*
- ³⁸*Affiliated with an institute covered by a cooperation agreement with CERN*
- ³⁹*ICCUB, Universitat de Barcelona, Barcelona, Spain*
- ⁴⁰*Instituto Galego de Física de Altas Enerxías (IGFAE), Universidade de Santiago de Compostela, Santiago de Compostela, Spain*
- ⁴¹*Instituto de Física Corpuscular, Centro Mixto Universidad de Valencia—CSIC, Valencia, Spain*
- ⁴²*European Organization for Nuclear Research (CERN), Geneva, Switzerland*
- ⁴³*Institute of Physics, Ecole Polytechnique Fédérale de Lausanne (EPFL), Lausanne, Switzerland*
- ⁴⁴*Physik-Institut, Universität Zürich, Zürich, Switzerland*
- ⁴⁵*NSC Kharkiv Institute of Physics and Technology (NSC KIPT), Kharkiv, Ukraine*
- ⁴⁶*Institute for Nuclear Research of the National Academy of Sciences (KINR), Kyiv, Ukraine*
- ⁴⁷*University of Birmingham, Birmingham, United Kingdom*
- ⁴⁸*H.H. Wills Physics Laboratory, University of Bristol, Bristol, United Kingdom*
- ⁴⁹*Cavendish Laboratory, University of Cambridge, Cambridge, United Kingdom*
- ⁵⁰*Department of Physics, University of Warwick, Coventry, United Kingdom*
- ⁵¹*STFC Rutherford Appleton Laboratory, Didcot, United Kingdom*
- ⁵²*School of Physics and Astronomy, University of Edinburgh, Edinburgh, United Kingdom*
- ⁵³*School of Physics and Astronomy, University of Glasgow, Glasgow, United Kingdom*
- ⁵⁴*Oliver Lodge Laboratory, University of Liverpool, Liverpool, United Kingdom*
- ⁵⁵*Imperial College London, London, United Kingdom*
- ⁵⁶*Department of Physics and Astronomy, University of Manchester, Manchester, United Kingdom*
- ⁵⁷*Department of Physics, University of Oxford, Oxford, United Kingdom*
- ⁵⁸*Massachusetts Institute of Technology, Cambridge, Massachusetts, USA*
- ⁵⁹*University of Cincinnati, Cincinnati, Ohio, USA*
- ⁶⁰*University of Maryland, College Park, Maryland, USA*
- ⁶¹*Los Alamos National Laboratory (LANL), Los Alamos, New Mexico, USA*
- ⁶²*Syracuse University, Syracuse, New York, USA*
- ⁶³*School of Physics and Astronomy, Monash University, Melbourne, Australia
(associated with Department of Physics, University of Warwick,
Coventry, United Kingdom)*
- ⁶⁴*Pontifícia Universidade Católica do Rio de Janeiro (PUC-Rio), Rio de Janeiro, Brazil
(associated with Institution Universidade Federal do Rio de Janeiro (UFRJ),
Rio de Janeiro, Brazil)*
- ⁶⁵*Physics and Micro Electronic College, Hunan University, Changsha City, China
(associated with Institute of Particle Physics, Central China Normal University,
Wuhan, Hubei, China)*
- ⁶⁶*Guangdong Provincial Key Laboratory of Nuclear Science, Guangdong-Hong Kong Joint Laboratory of
Quantum Matter, Institute of Quantum Matter, South China Normal University, Guangzhou, China
(associated with Center for High Energy Physics, Tsinghua University, Beijing, China)*
- ⁶⁷*Lanzhou University, Lanzhou, China
(associated with Institute of High Energy Physics (IHEP), Beijing, China)*
- ⁶⁸*School of Physics and Technology, Wuhan University, Wuhan, China
(associated with Center for High Energy Physics, Tsinghua University, Beijing, China)*
- ⁶⁹*Departamento de Física, Universidad Nacional de Colombia, Bogota, Colombia
(associated with LPNHE, Sorbonne Université, Paris Diderot Sorbonne Paris Cité, CNRS/IN2P3,
Paris, France)*
- ⁷⁰*Universität Bonn—Helmholtz-Institut für Strahlen und Kernphysik, Bonn, Germany
(associated with Physikalisches Institut, Ruprecht-Karls-Universität Heidelberg, Heidelberg, Germany)*
- ⁷¹*Eotvos Lorand University, Budapest, Hungary
(associated with European Organization for Nuclear Research (CERN), Geneva, Switzerland)*

⁷²*INFN Sezione di Perugia, Perugia, Italy*
(associated with Institution INFN Sezione di Ferrara, Ferrara, Italy)
⁷³*Van Swinderen Institute, University of Groningen, Groningen, Netherlands*
(associated with Nikhef National Institute for Subatomic Physics, Amsterdam, Netherlands)
⁷⁴*Universiteit Maastricht, Maastricht, Netherlands*
(associated with Nikhef National Institute for Subatomic Physics, Amsterdam, Netherlands)
⁷⁵*DS4DS, La Salle, Universitat Ramon Llull, Barcelona, Spain*
(associated with ICCUB, Universitat de Barcelona, Barcelona, Spain)
⁷⁶*Department of Physics and Astronomy, Uppsala University, Uppsala, Sweden*
(associated with School of Physics and Astronomy, University of Glasgow, Glasgow, United Kingdom)
⁷⁷*University of Michigan, Ann Arbor, Michigan, USA*
(associated with Syracuse University, Syracuse, New York, USA)

^aDeceased.

^bAlso at Università di Firenze, Firenze, Italy.

^cAlso at Scuola Normale Superiore, Pisa, Italy.

^dAlso at Università di Ferrara, Ferrara, Italy.

^eAlso at Università di Milano Bicocca, Milano, Italy.

^fAlso at Università di Bologna, Bologna, Italy.

^gAlso at Università di Genova, Genova, Italy.

^hAlso at Universidad Nacional Autónoma de Honduras, Tegucigalpa, Honduras.

ⁱAlso at Università di Bari, Bari, Italy.

^jAlso at Università di Cagliari, Cagliari, Italy.

^kAlso at Università di Roma Tor Vergata, Roma, Italy.

^lAlso at Universidade de Brasília, Brasília, Brazil.

^mAlso at Hangzhou Institute for Advanced Study, UCAS, Hangzhou, China.

ⁿAlso at Università di Siena, Siena, Italy.

^oAlso at Università degli Studi di Milano, Milano, Italy.

^pAlso at Central South University, Changsha, China.

^qAlso at Università di Padova, Padova, Italy.

^rAlso at Università di Perugia, Perugia, Italy.

^sAlso at Excellence Cluster ORIGINS, Munich, Germany.

^tAlso at Università di Pisa, Pisa, Italy.

^uAlso at Università della Basilicata, Potenza, Italy.

^vAlso at Universidad de Alcalá, Alcalá de Henares, Spain.

^wAlso at Università di Urbino, Urbino, Italy.